2018

# Numerical Simulations of Perforated Nozzle Inlets for Ramjets

Chuwei Chen
*Lehigh University*, mvproy7@gmail.com

# Numerical Simulations of Perforated Nozzle Inlets for Ramjets

by

Chuwei Chen

A Thesis

Presented to the Graduate and Research Committee

of Lehigh University

in Candidacy for the Degree of

Master of Science

in

Mechanical Engineering and Mechanics

Lehigh University

April 2018

This thesis is accepted and approved in partial fulfillment of the requirements for the Master of Science.

_____

Date

_____

Thesis Advisor

_____

Chairperson of Department

# Acknowledgements

I would like to appreciate everyone who helped me in this research. First I want express my best thankfulness to my advisor, Prof. Alparslan Oztekin, for all his efforts, especially for him being patience when I faced difficulties in the first few months. Second I would like to thank Trevor Hayes. He came up with brilliant idea of doing research on perforated inlet diffuser for ramjet. I'm also grateful to Guanyang Xue, for his selfness helps in OpenFOAM. Furthermore I want to thank my family, for their continuous encouragement and support during my research.

# Contents

# List of Tables

# List of Figures

# Abstract

Computational fluid dynamics simulations of supersonic flows through perforated and non-perforated nozzles are conducted. The primary objective of this thesis is to examine the influence of perforations in the convergent section of the nozzle on the spatial and temporal characteristics of the supersonic flows inside and outside the nozzle. The perforated nozzle might be utilized as supersonic inlet diffuser for high-speed flight engines, like ramjet, to reduce huge total pressure loss at starting process. The nozzle design is crucial for overall design of these systems, and the solution investigated here enjoys a high degree of interest for over 50 years.Open source CFD tool OpenFoam is used in this research. Two compressible solvers named the *sonicFoam* and *rhoCentralFoam* are introduced and used. To validate the mathematical model and numerical methods, simulations are conducted for supersonic flows over 23 degree wedge at Mach number 1.5 and flow over 2.86 degree wedge at Mach number 1.6. The pressure and velocity field and the characteristics of the oblique shock are determined and are compared against the results of the analytical solution. The predicted and analytical solution for the location and the pressure ratio matches well; validating the mathematical model and the numerical method employed. Simulations for supersonic flows through non-perforated and perforated nozzle are performed for a range of Mach number from 1.2 to 2.0. The total pressure is set to the same value for all simulations. Discretization is made using the *sonicFoam* and *rhoCentralFoam* solver. In order to characterize the flow images of the velocity field are presented for various values of Mach number. It is demonstrated that the bow shock is moved into the nozzle or is swallowed by the nozzle in the perforated nozzle geometry when incoming flow Mach number exceeds 1.8.

The comparing of total pressure recovery ratio also demonstrated that the perforation can reduce the total pressure loss as the bow shock is swallowed. Our results in the perforated and non-perforated nozzle geometry agree well with the results reported and documented in the literature. This study aids designing and optimizing of the ramjet intake diffuser. This study also demonstrates that the OpenFoam can effectively be used to characterize the supersonic flow field in a complex geometry.

# Chapter 1

# Introduction

## 1.1 Background

Ramjet propulsion began to attract interest toward 1940s when the turbojet was the most effective method of achieving high flight speed. In this period it was also believed that ramjet engine would be a next step for obtaining higher flight speed. Ramjet takes advantage of its forward motion to compress free stream air by methods of a simple convergent nozzle rather than multistage compressors typically required in turbojet engine[1]. The incoming flow over the compression stage of the turbojet engine is limited to subsonic speed because axial compressors could not operate properly when the flow over the fan airfoils reaches supersonic speeds. The inlets of turbojet are required to be designed to slow the supersonic free stream to subsonic, and this is often accomplished this by forming oblique shocks at or in front of the engine inlet. Ramjet engines have no such design requirements, but ramjet combustor still requires subsonic incoming flow.

Decelerating a supersonic flow to subsonic speeds might be accomplished by introducing a shock into the system associated with this discontinuous process is a decrease in total pressure[2]. Deceleration from supersonic to subsonic flow velocity can be done by a normal shock with small total pressure loss if the incoming flows Mach number is close to 1. For high Mach number, Mach number $\gg 1$, the loss across a normal shock would be excessive;

in this case, a combination of oblique shock and normal shock would be a better solution.

The convergent-divergent type diffuser investigated by Kantrowitz and Donaldson[3] and by Wyatt and Hunczak[4] is another method to obtain subsonic flow when ramjet is operating at supersonic speed. This kind of diffuser appears like a reversed supersonic nozzle which would be the ideal device to produce isentropic deceleration. Unfortunately, this flow behavior is heavily dependent on the coupling between incoming flow velocity and the geometry of the convergent-divergent nozzle and subsequent engine sections.

When reverse nozzle diffuser operates in subsonic condition, mass is not choked at the minimum cross-section of the diffuser (most time at throat), and the upstream capture area $A_t$ is determined by downstream of the inlet. At this speed, the diffuser operates well and flow in the diffuser is isentropic. Since the flow is assumed to be isentropic, then the capture area $A_a$ is given by equation[5]:

$$\frac{A_a}{A_t} = \frac{1}{M}\left[\frac{2}{\gamma+1}\left(1+\frac{\gamma-1}{2}M^2\right)\right]^{\frac{\gamma+1}{2(\gamma-1)}}$$

From this equation, it is easily found that for sufficiently high subsonic values of Mach number or supersonic speed, the capture area would be less than the inlet area. At these conditions, the entrance mass flow will not pass through the throat of the diffuser, choking will occur, and therefore spillage will appear around the inlet. The spilled air must be reduced to subsonic velocity upstream of the inlet plane to sense the presence of the inlet and flow around it. The mechanism for this deceleration is a detached bow shock that stands sufficiently far upstream to allow the required spillage. This mechanism is necessarily non-isentropic.

In order to achieve isentropic flow deceleration in a reverse nozzle diffuser, over- speeding is one of many approaches[6]. From the equation (1.1) displayed above, when incoming flow Mach number is sufficiently high, the ratio of upstream capture area to diffuser minimum area became larger, and once this ratio is larger than the ratio of diffuser inlet area to the throat area, bow shock will be swallowed and the isentropic flow will be established. Most ramjet applications, however, are required to operate over a wide range of flight Mach

numbers. Establishing this inlet flow behavior is thus very difficult in what called Starting Conditions where the free stream Mach number is much lower than the optimal design point.

If over speeding is not feasible, bow shock might be possible to be swallowed by a variation of nozzle geometry at a constant speed[7][8][9]. Assume the incoming flow is accelerated to the design Mach number with the bow shock present. At this moment, if the actual area can be decreased from Ai/At to the value that can ingest the entire inlet flow behind the shock, the shock will be swallowed, and isentropic flow will be established. This ratio variation would be achieved by a momentary increase of the throat area. However, achieving rapid, precise, stable geometric variation in a supersonic diffuser would be difficult, tedious, and expensive at the 1950s[10].

Drilling a succession of holes or perforations in the diffuser can achieve a similar effect as a variation of geometry. The perforated diffuser can let part of the subsonic mass flow entering the inlet pass through the perforations, the flow spilled over the inlet will decrease, and the shock will move nearer to the inlet[11][12][13].

As the shock is swallowed by the diffuser, the supersonic flow will be established in the convergent inlet. The static pressure difference between external and internal flow will decrease. Likewise, the holes become less effective as the incoming flow Mach number increases because the high-velocity flow has less time to swerve and pass through the holes. These two factors tend to reduce the loss of mass flow through the perforations as compared with operating at a subsonic speed. Thus, the perforations operate as automatic valves, which are open during low Mach number speed or starting process and partly closed during operation speed. Comparing to the variation of throat area at specific speed, the perforated diffuser is much practicable.

## 1.2 Motivation

The purpose of this thesis is to investigate the effectiveness of perforations in the convergent section of the nozzle inlet in allowing the bow shock. In the 1950s, validation of this

design required tests in the supersonic wind tunnel, and it would be prohibitively expensive. However, numerical simulations can be effectively used for design evaluations and validation thus obviating the need for expensive wind tunnel test. Although there are several commercial CFD software available today, many supersonic simulations are performed by open source solvers such as CFD3D[14] and Solver II[15]. An open source CFD package, namely OpenFOAM, is used in this thesis. Being an open source tool, it provides with greater flexibility in customization and gives individual non-commercial users a chance to do simulations and research free. As research and application of compressible solvers in OpenFOAM are rare, the validation test is conducted using several 2-dimensional models of wedge.

# Chapter 2

# Mathematical Model and Numerical Method

## 2.1 Governing Equations

The equations governing the supersonic flows are:

Conservation of mass:

$$\frac{\partial \rho}{\partial t} + \nabla \cdot [u\rho] = 0 \tag{2.1}$$

Conservation of momentum:

$$\frac{\partial (\rho u)}{\partial t} + \nabla \cdot [u (\rho u)] + \nabla p + \nabla \cdot T = 0 \tag{2.2}$$

Conservation of total energy:

$$\frac{\partial (\rho E)}{\partial t} + \nabla \cdot [u (\rho E)] + \nabla \cdot [up] + \nabla \cdot [T \cdot u] + \nabla \cdot j = 0 \tag{2.3}$$

Where $\rho$ is the mass density, $u$ is the fluid velocity, $p$ is the pressure; $j$ is the diffusive flux of heat and $T$ is the viscous stress tensor. Simulation in this thesis is inviscid, hence $T = 0$.

The diffusive flux of heat can be represented by Fouriers law:

$$j = -k\nabla T \tag{2.4}$$

Where $T$ is the temperature and $k$ is the conductivity. And $k$ is same in all directions as we assumed all simulations were ran in isotropic condition.

In equation (2.3),$E$ is the total energy density:

$$E = e + \frac{|u|^2}{2} \tag{2.5}$$

Where $e$ is the specific internal energy and defined by:

$$e = C_v T = (\gamma - 1)\, RT \tag{2.6}$$

### 2.1.1 Boundary Conditions

#### 23 Degree Wedge

23 degree wedge is introduced for validation of solvers as displayed in Figure 3.1. The 23 degree wedge obstacle is defined as type *wall*. The inlet, outlet and top boundary are set to type *patch*. The bottom boundary before the 23 degree wedge obstacle is set to *symmetryPlane* to reduce simulation time.

**Inlet** At the inlet,$p$, $T$ and $U$ fully defined the flow. $FixedValue$ boundary is used to define value of $p$, $T$ and $U$.

$$Q = fixedValue \tag{2.7}$$

Where $Q$ denotes the pressure, velocity and temperature. The inlet temperature is chosen as 298K. This gives a speed of sound of 346m/s. Therefore, for Mach 1.5, the stream-wise velocity at the inlet is 543m/s. The set pressure value at the inlet in the inviscid flow does not influence the flow field, and the pressure is set to approximately 81.1kPa. However, in a viscous flow simulation, the pressure would be the parameter used to control the Reynolds

number for a specified fluid viscosity.

**Outlet** At the outlet, the *zeroGradient* condition is imposed. The value of the flow parameters on the face will be assumed to be the same as value of the first cell within the domain. For an outlet in supersonic flows the zeroGradient condition is usually an appropriate boundary condition, and it is applied more commonly to simulate supersonic compressible flows.

$$\frac{\partial Q}{\partial n} = 0 \tag{2.8}$$

Where $Q$ denotes the pressure, velocity and temperature.

**Obstacle** Since the flow is assumed to be inviscid, the slip condition is used for the velocity field. In OpenFOAM, the slip boundary condition is defined as:

$$\overrightarrow{U_p} = \overrightarrow{U_c} - \left(\overrightarrow{U_c} \cdot \vec{n}\right) \vec{n} \tag{2.9}$$

Where $\overrightarrow{U_p}$ is the velocity at boundary and $\overrightarrow{U_c}$ is the velocity at the nearest grid center and $\vec{n}$ is unit normal vector at boundary.

Pressure and temperature are set to zeroGradient on the surface of obstacle which is introduced in equation 2.8

**Bottom Flat Surface** Since the flow is symmetrical, along the flat surface at the bottom, a *symmetryPlane* boundary condition is used for $p$,$T$ and $U$.

### 2.86 Degree Wedge

2.86 degree wedge is introduced for validation of solvers as displayed in Figure 3.3.Simulation setup of 1.6 Mach supersonic flow over 2.86 degree wedge is similar as case of 23 degree wedge above. Differences between these two cases is that inlet velocity in case of 2.86 degree wedge is set to 553.6m/s (M=1.6).

**Diffusers**

As shown in Figure 3.5 and 3.6. The diffuser is defined as type *wall*. The inlet, outlet and top boundary are set to type *patch*. The bottom boundary is set to *symmetryPlane* to reduce simulation time.

**Inlet** In case of flow over wedge, boundary condition on the inlet is set to $fixedValue$ which is similar as boundary condition in supersonic flow tutorial. However, after reading source code of boundary conditions, $Freestream$ boundary might be a better solution. $Freestream$ boundary is like a hybrid $fixedValue$ and $zeroGradient$ boundary condition. It behaves like a $zeroGradient$ when fluid is flowing out of the boundary face, but behaves like a $fixedValue$ when fluid is not flowing out. Unlike $fixedValue$ boundary that imposes its constant value regardless of situation, $Freestream$ boundary is more flexible and more physically realistic.

$$\begin{aligned} Q &= refValue, && \text{inflow} \\ \tfrac{\partial Q}{\partial n} &= 0, && \text{outflow} \end{aligned} \tag{2.10}$$

Where $Q$ denotes the pressure, velocity and temperature.

**Outlet** Setting the outlet and top as $zeroGradient$ in supersonic flow is usually an appropriate boundary condition. However, considering ramjet operating in supersonic free stream, this BC will mess up the simulation results by reflecting of shock wave on boundary. To prevent the occurrence of a reflection wave, a special outlet BC $waveTransmissive$ is applied. $WaveTransmissive$ BC provides an advective outflow condition based on solving:

$$\frac{D\left(psi, U\right)}{Dt} = 0 \tag{2.11}$$

Where $U$ is the wave velocity at the boundary. The temperature at this boundary is set to $zeroGradient$.

**Diffuser** As for the flow is inviscid, the diffuser is set to *slip* condition as displayed in equation 2.9. Pressure and temperature are set to *zeroGradient* which is introduced in equation 2.8.

**Bottom** Since the flow is symmetrical, a *symmetryPlane* boundary condition is used for $p$, $T$ and $U$ on the bottom boundary.

### 2.1.2 Initial Conditions

Initial conditions are essentially unimportant because they will not affect the steady state solution. However, if these initial conditions are too extreme, the convergence would be slower, or simulations would even diverge. The pressure is set lower than the inlet pressure, the temperature equal to the inlet temperature, and the velocity is set to 0 as initial conditions.

## 2.2 Numerical Methods

Two solvers in OpenFOAM are available to solve supersonic air flow problems. *SonicFoam* is a pressure based solver uses pressure and velocity as dependent variable through PIMPLE method. *rhoCentralFoam* is a density based solver with central-upwind schemes.

### 2.2.1 *sonicFoam*

The momentum equation (2.2) is discretized as[16]

$$\int\int \frac{\partial u}{\partial t}\mathrm{d}V\mathrm{d}t = (u_p^r - u_p^n)V_p \tag{2.12}$$

$$\int\int \nabla\cdot(u\otimes u)\mathrm{d}V\mathrm{d}t = \int\int u\otimes u\mathrm{d}S\mathrm{d}t = \sum(\Phi^n u_f^r)\Delta t \tag{2.13}$$

$$\begin{aligned}\int\int \nabla\cdot(\nu\nabla u)\mathrm{d}V\mathrm{d}t &= \int\int \nu\nabla\ u\mathrm{d}S\mathrm{d}t \\ = \sum \nu(\nabla u^r)_f \boldsymbol{S}_f\Delta t &= \sum\left(\nu|\boldsymbol{S}_f|\frac{u_N^n - u_P^n}{|d|}\right)\Delta t\end{aligned} \tag{2.14}$$

where superscript $^n$ is the current time step and superscript $^r$ denotes the predicted time step. Subscript $_f$ represents the value on cell surface, subscripts $_P$ and $_N$ represent the present and the neighboring cells, respectively.

Substitute the discretization properties into the momentum equation:

$$\frac{u_p^r - u_p^n}{\delta t} V_p + \sum \left( \Phi^n u_f^r \right) = \sum \nu |S_f| \frac{u_N^n - u_p^n}{|d|} - \nabla p^n \tag{2.15}$$

Interpolate the velocity on a cell surface by central differencing scheme:

$$u_f^r = \frac{u_P^r - u_N^r}{2} \tag{2.16}$$

Then,

$$A_p u_p^r + \sum A_n u_N^r - E_P^n = -\nabla p^n \tag{2.17}$$

where

$$\begin{aligned} A_P &= \frac{V_p}{\Delta t} + \sum \frac{\Phi_f^n}{2} + \sum \left( \nu \frac{|\boldsymbol{S}_f|}{|d|} \right) \\ A_N &= \frac{\Phi_f^n}{2} - \nu \frac{|\boldsymbol{S}_f|}{|d|} \\ E_P &= \frac{V_P}{\Delta t} u_P^n \end{aligned} \tag{2.18}$$

We can get predicted velocity $u_P^r$:

$$u_P^r = \frac{1}{A_P} (- \sum A_n u_N^r + E_P^n - \nabla p^n) \tag{2.19}$$

The velocity field $u^r$ does not satisfy the continuity equation. We need derive a corrected velocity field $u^{n+1}$ through pressure equation. Combine equation (2.18) and equation (2.1):

$$\frac{\partial \rho}{\partial t} + \nabla \cdot (\rho u A_p) - \nabla \cdot \left( \rho \frac{1}{A_p} \nabla p \right) = 0 \tag{2.20}$$

Substitute $\rho = \psi p$, finally get:

$$\frac{\partial \psi p}{\partial t} + \nabla \cdot (\psi p u_P^r A_P) - \nabla \cdot \left( \psi p \frac{1}{A_P} \nabla p \right) = 0 \tag{2.21}$$

**Algorithm**

PIMPLE algorithm is a combination of SIMPLE and PISO. PIMPLE algorithm has three loops: outer SIMPLE loop, middle PISO loop and inner nonorthogonal correct loop, as shown in Figure 2.1[17]. In PIMPLE, it first searches a steady solution with under-relaxation as SIMPLE correction in outer loop. After the tolerance is reached we use PISO correction to calculate the time derivative term as the inner loop[18].

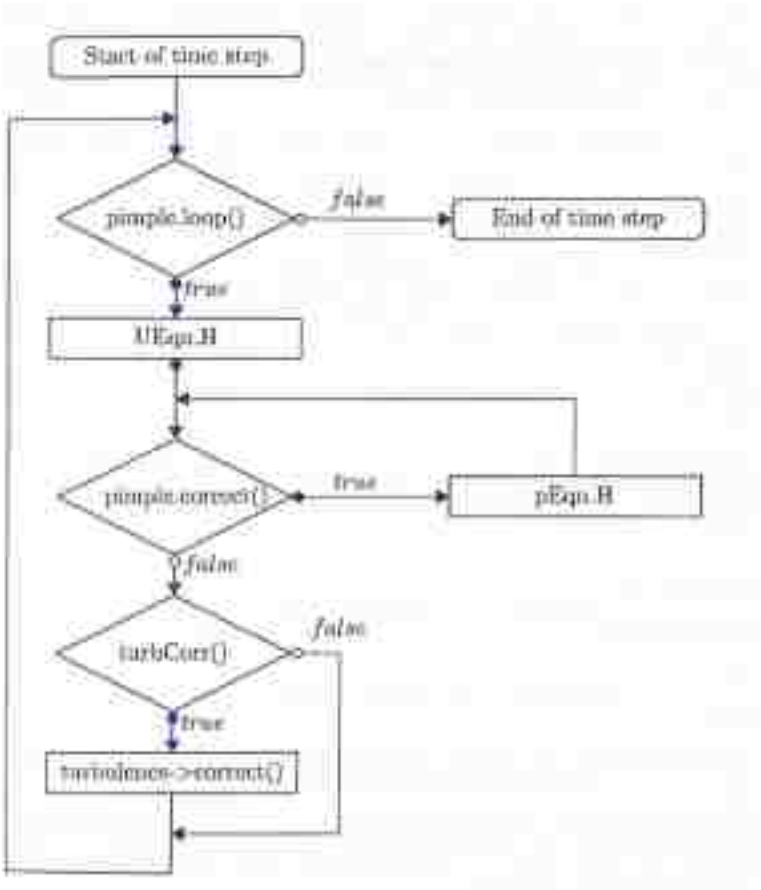


Figure 2.1: OpenFOAM PIMPLE Algorithm Flow Chart

In sonicFoam, there are slight differences compared to the version shown in Figure 2.1. An energy equation, $EEqn.H$, which is tackled right after the momentum predictor, $UEqn.H$, and before the corrector loop.

If we have a look at code of $sonicFoam$[19], we can get basic algorithm like:

| Algorithm 1 $sonicFoam$ |
|---|
| ***Outer*** $pimple.loop()$ (similar as SIMPLE loop) |
| Use current u, solve u equation (2.18) |
| Solve energy equation (2.3) and evaluate T |
| ***Middle*** $pimple.correct()$ (almost same as PISO loop) |
| Construct $rAU$ and $HbyA$ by u |
| Use $HbyA$ bulids $PhiHbyA$ and add $fvc :: ddtCorr(u, phi)correct$ |
| $adjustPhi()$ |
| Add consistent correct to $phiHbyA$ |
| $constrainPressure()$ |
| ***Inner*** $pimple.correctNonOrthogonal()$ (non-orthogonal correct) |
| Define and solve pressure equation (2.21) |
| $pEqn.setReference()$ |
| Use new p as initial value solve pressure equation and do non-orthogonal correct |
| Update u,Phi,K and density |

Table 2.1: Algorithm of $sonicFoam$

### 2.2.2 *rhoCentralFoam*

$rhoCentralFoam$ applies an alternative approach to Riemann solvers based on central-upwind schemes. Methods of Central schemes implemented in $rhoCentralFoam$ are Kurganov method[20] and Kurganov and Tadmor method[21].

The convective terms of conservation equation in equation (2.1-3) like $\nabla \cdot [u(\rho u)]$ are integrated over a control volume and linearized as follows[22]:

$$\int_V \nabla \cdot [u\psi] \, \mathrm{d}V = \sum_f [S_f \cdot u_f] \, \psi_f \approx \sum_f \phi_f \psi_f \tag{2.22}$$

Where $\sum_f$ is summation over all faces and $\phi_f$ is the volumetric flux. $\psi_f$ is obtained by

splitting the flux in outgoing and incoming to the face directions.

$$\sum_f \phi_f \psi_f = \sum_f \left[\alpha \phi_{f+} \psi_{f+} + (1-\alpha)\, \phi_{f-} \psi f - + \omega_f \left(\psi_{f-} - \psi_{f+}\right)\right] \tag{2.23}$$

where $f_+$ and $f_-$ denote directions coinciding with the directions $+S_f$ and $-S_f$, respectively. Then, volumetric fluxes associated with the local speed of propagation can be calculated as [23]:

$$\begin{aligned} \phi_{f+} &= max\left(\alpha_{f+}|S_f| + \phi_{f+}, \alpha_{f-}|S_f| + \phi_{f-}, 0\right) \\ \phi_{f-} &= max\left(\alpha_{f+}|S_f| - \phi_{f+}, \alpha_{f-}|S_f| - \phi_{f-}, 0\right) \end{aligned} \tag{2.24}$$

Where $\alpha_{f\pm}$ are the speeds of sound of gas at the face. The scheme is termed central if the weight coefficient of $f_+$ and $f_-$ contributions is =0.5; Schemes on which the weighting is biased in the upwind direction by means of $\alpha = \frac{\psi_{f+}}{(\psi_{f_+} - \psi_{f-})}$ are central upwind. The diffusive volumetric flux term:

$$\omega_f = \begin{cases} \alpha max(\phi_{f+}, \phi f -, & \text{Kurganov and Tadmor scheme} \\ \alpha(1-\alpha)(\phi_{f+} + \phi_{f-}), & \text{Kurganov scheme} \end{cases} \tag{2.25}$$

To switch between first and second order schemes, the interpolation procedure uses a flux limiter function $\beta(r)$,where r represents the ratio of successive gradient of the interpolated variable.

$$\beta_r = \begin{cases} \frac{r+|r|}{1+r}, & \text{VanLeer} \\ \frac{r+r^2}{1+r^2}, & \text{VanAlbada} \\ max(0, min(1, r)), & \text{Minmod} \end{cases} \tag{2.26}$$

As for gradient terms, these terms are integrated over a volume and discretized as

$$\int_V \nabla \psi \mathrm{d}V = \int_S \mathrm{d}S \psi \approx \sum_f S_f \psi_f \tag{2.27}$$

Then splitting the interpolation procedure into $f_+$ and $f_-$:

$$\sum_f S_f \psi_f = \sum_f [\alpha S_f \psi_{f+} + (1-\alpha) S_f \psi_{f-}] \tag{2.28}$$

Laplacian terms are not presented because this thesis runs simulations for inviscid supersonic flow.

**Algorithm**

After getting equations above, we can easily understand the algorithm for *rhoCentralFoam* from source code[23]. *rhoCentralFoam* solves density-weighted fields: $\rho$ , momentum density $\overset{\wedge}{u} = \rho u$ , and total energy density $\overset{\wedge}{E} = \rho E$ [22].

| Algorithm 2 *rhoCentralFoam* |
|---|
| ***while*** t<$t_{end}$ ***do*** |
| Set t:=t+$\Delta t$ |
| Use limiter evaluate $\rho_{f\pm}$,$u_{f\pm}$,$T_{f\pm}$ from $\rho$,u and T |
| Calculate $u_{f\pm} = u^{\wedge}_{f\pm}/\rho_{f\pm}$, $p_{f\pm} = \rho_{f\pm} R T_{f\pm}$, $\phi_{f\pm} = S_f \cdot u_{f\pm}$, $c_{f\pm} = \sqrt{\gamma R T_{f\pm}}$ |
| Calculate convective derivatives and $\nabla p$ from $f\pm$ interpolates using equations (2.22-2.28) |
| Update $T_{exp}$, $\mu$ and k |
| Solve equation (2.1) for $\rho$ {density equation} |
| Solve equation (2.2) for $\overset{\wedge}{u}$ {momentum equation} |
| Update u from $\overset{\wedge}{u}$ and $\rho$ |
| Solve equation (2.3) for $\overset{\wedge}{E}$ {energy equation} |
| Update T by equation (2.5) from $\overset{\wedge}{E}$, u and $\rho$ |
| Update p by $p = \rho R T$ |
| ***end while*** |

Table 2.2: Algorithm of *rhoCentralFoam*

# Chapter 3

# Geometry and Computational Domain

Several models are introduced in this chapter. 23 degree wedge and 2.86 degree wedge are designed for validating compressible solvers in OpenFOAM. Perforated diffuser and non-perforated diffuser are used to investigate the effectiveness of perforations in the convergent section of the nozzle inlet in allowing the bow shock.

## 3.1 Validation Simulations

### 3.1.1 23 Degree Wedge

The geometry of 23 degree wedge is shown in Figure 3.1.

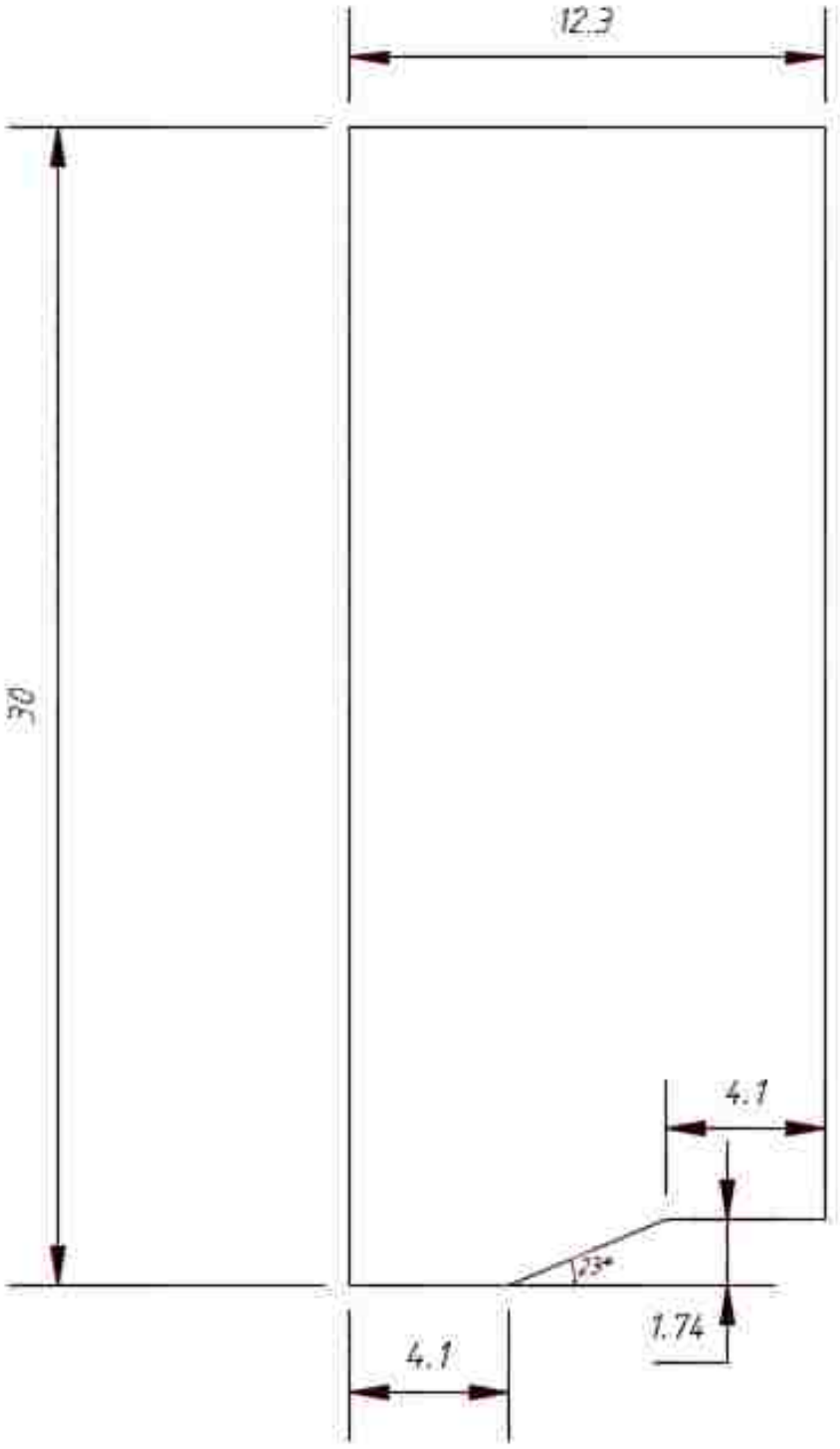


(a)

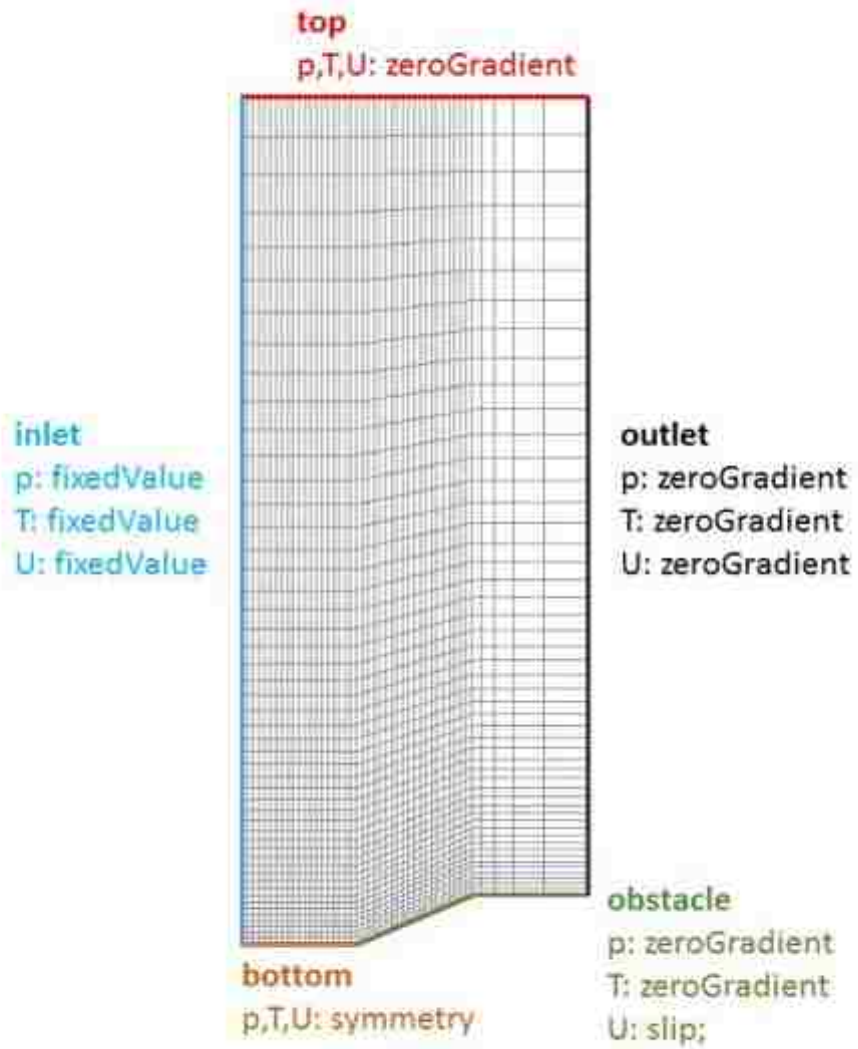


(b)

Figure 3.1: Geometry and Mesh of 23 degree Wedge. (a) is geometry of wedge and (b) is mesh of wedge, boundary conditions are also presented in (b).

Considering relatively simple geometry, the mesh is generated by the native OpenFOAM meshing tool *blockMesh*. *BlockMesh* uses vertices to define the geometry of model and blocks to define the different regions within the mesh. Considering simple geometry, blocks are split up to 3 parts[24] and mesh is refined in blocks close to wedge, as shown in Figure

3.1.

Boundaries are defined in *blockMesh* too. The 23 degree wedge obstacle is defined as type *wall*. The inlet, outlet and top boundary are set to type *patch*. The bottom boundary before the 23 degree wedge obstacle is set to *symmetryPlane* to reduce simulation time.

### 3.1.2 2.86 Degree Wedge

The geometry of 2.86 degree wedge is shown in Figure 3.2.

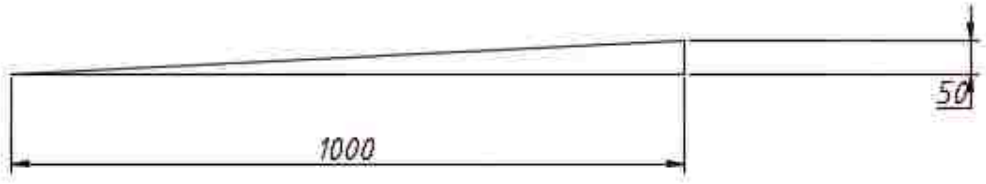


Figure 3.2: Geometry of 2.86 degree wedge

Unlike simple 23 degree wedge, the sharp angle of wedge is hard to deal in pre-processing command in OpenFOAM.

Y-Block in ICEM CFD is introduced to generated mesh in this case. At the same time, ICEM CFD gives more freedom of refining mesh which makes structure mesh generated in ICEM CFD has better quality and able to reduce cell numbers. Mesh is refined around the wedge where $\Delta x \approx 2.5mm$ , then gradually increased mesh size to boundary with expansion ratio of 1.02. One thing need mention is that the mesh inside wedge will be delete because no flow motion inside wedge. The Mesh of 2.86 degree wedge is shown in Figure 3.3.

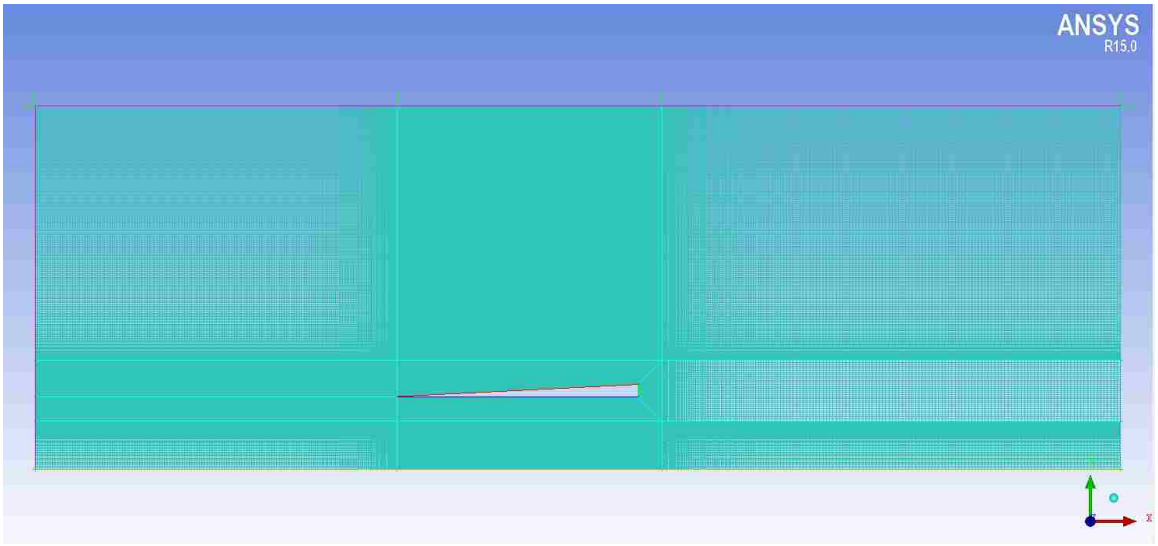


(a)

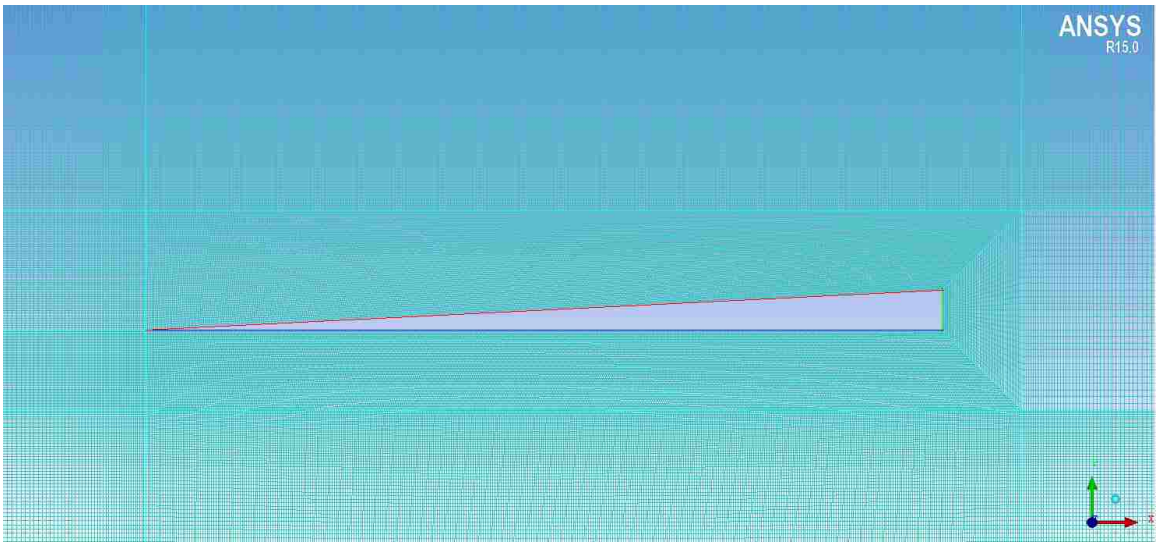


(b)

Figure 3.3: Mesh of 2.86 degree wedge. (a) is the mesh of whole computational domain and (b) show detailed mesh near wedge.

## 3.2 Diffuser

The geometry pictured in Figure 3.4 generated the basic shape of the axially symmetric ramjet where all units are measured in millimeters. The inlet features a capture to throat area of approximately 1.5 and the engine sports a generic nozzle at its rear which allows for the modeling of flow behavior in the combustion chamber. As for perforated diffuser, the perforations are simple 10mm diameter spaced 30mm apart along the length of the convergent portion of the inlet[25].

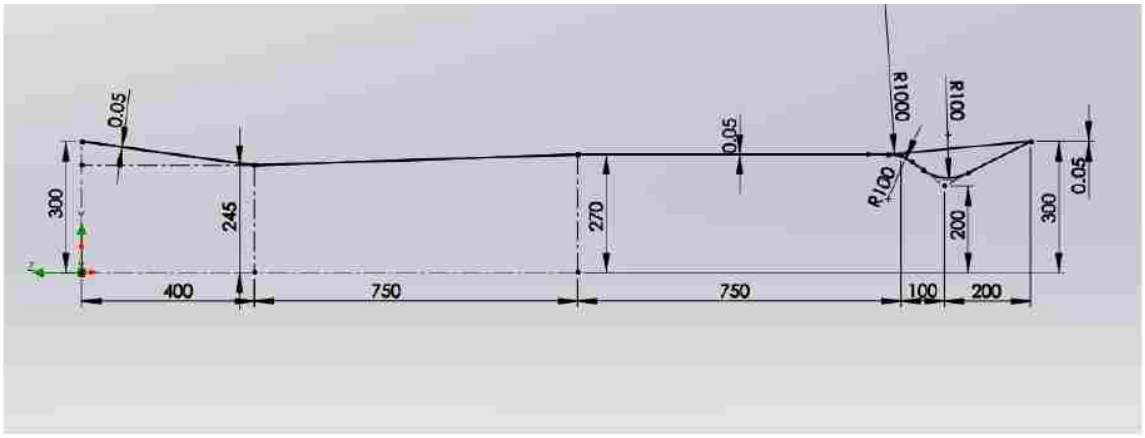


Figure 3.4: Geometry of Diffuser.

The geometry is built in Solidworks and output point data in text file. Then, importing point data in ICEM CFD and connecting points with lines. At the same time, simulation domain is established. The inlet set to 2 meters from the origin, outlet set to 3 meters from the origin and the top of domain set at 2.5 meters from X-axis.

Mesh of diffuser is generated by ICEM CFD too. Multi-blocks are built close to geometry to portray shape of diffuser. This block will be delete later because no flow motion inside diffuser wall. Diffuser is boxed in a 2500x400 block. Mesh in this block will refine to 2.5 mm. Outside this block, mesh size will gradually enlarge with expansion ratio of 1.02. Figure 3.5 shows mesh of the non-perforated diffuser and Figure 3.6 shows mesh of perforated diffuser.

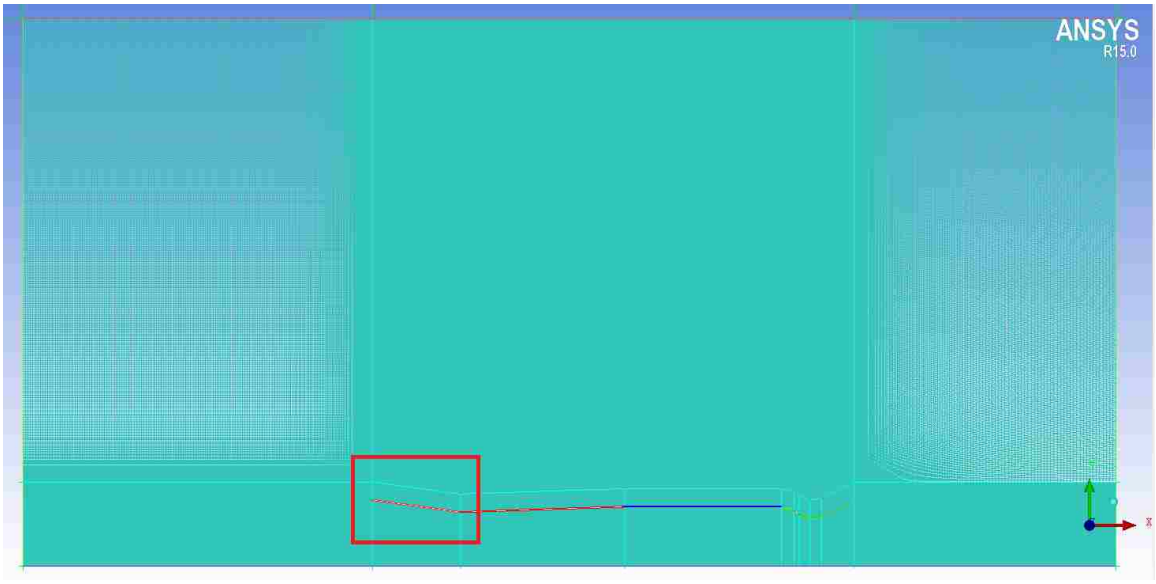


(a)


(b)

Figure 3.5: Mesh of Non-Perforated Diffuser. (a) is the mesh of whole computation domain for the supersonic flow over non-perforated nozzle. The detailed mesh at convergent section of non-perforated nozzle is presented in (b).

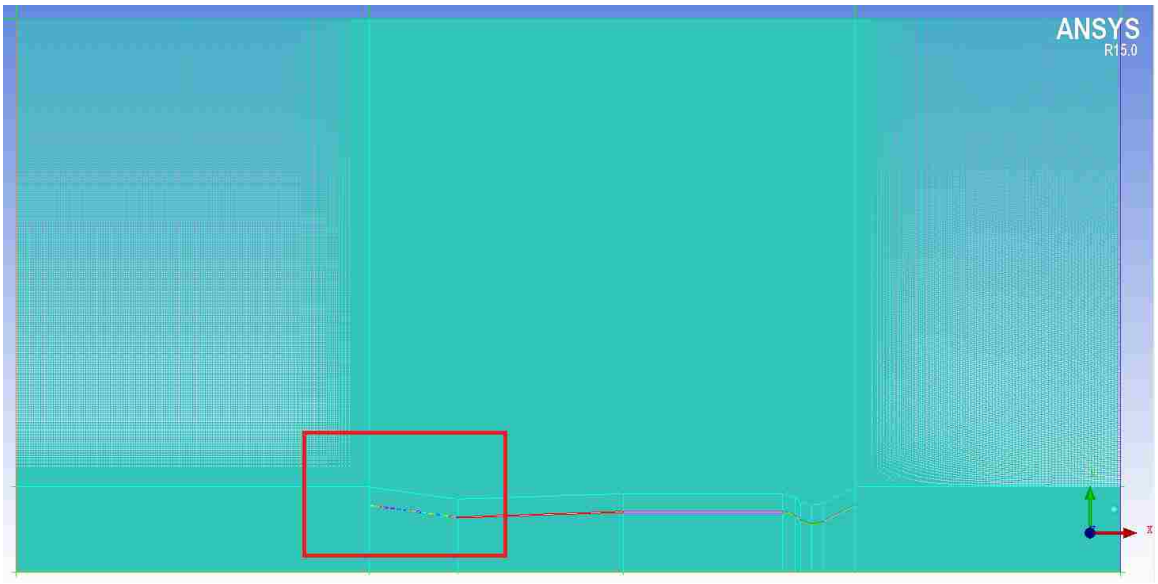


(a)


(b)

Figure 3.6: Mesh of Non-Perforated Diffuser. (a) is the mesh of whole computation domain for the supersonic flow over perforated nozzle. The detailed mesh at convergent section of perforated nozzle is presented in (b).

## 3.3 Mesh Optimization Study

Mesh study is divided into two parts for flow simulations with of the diffuser geometry. The first part is the refinement of mesh around the diffuser. The mesh in the region near the diffuser is refined to 5mm, 2.5mm, 1mm and 0.5 mm, respectively Considering the diameter of perforations and the thickness of the diffuser wall, the cell size is restricted to the size of the divisor which is 5mm long to avoid fragmenting mesh.

Figure 3.7 shows results of mass flow rate through the diffuser for four different grid sizes for incoming flow at Mach number 2. Mesh optimization simulations utilize the sonicFoam since the somniFoam requires greater resolution compared the centralFoam solver. It is observed that the difference between mesh refined among grid size of 2.5mm, 1mm, and 0.5mm is less than 1%. In order to save the computational resources, the refinement of mesh around the diffuser is set to 2.5mm.

The second part is the size of the computational domain. The distance between the inlet of the computational domain and the inlet of the diffuser should be sufficiently long to establish a bow shock at low Mach number supersonic flows. To optimize this distance, the inlet of the computational domain is set to 5m away from the diffuser inlet with the incoming flow at the lowest test speed considered. Locating the position of the bow shock by using the value of the centerline pressure we set inlet 0.1m away from the location of the shock. We define the wavetransmissive boundary condition at the outlet to minimize the reflection of shock, hence the location of the outlet is set to a safe distance away from the diffuser outlet. The outlet is set to 2m, 2.5m, 3m, 3.5m, 4m and 5m away from the throat of diffusers.These cases are simulated with the similar setup as above and results are shown in Figure 3.8. The mass flow rates at the outlet of the diffuser are practically independent of the location of the outlet of the computational domain when the distance between the outlet and the origin is larger than 2.5m. Hence, the outlet is set to 3 meters away from the origin.

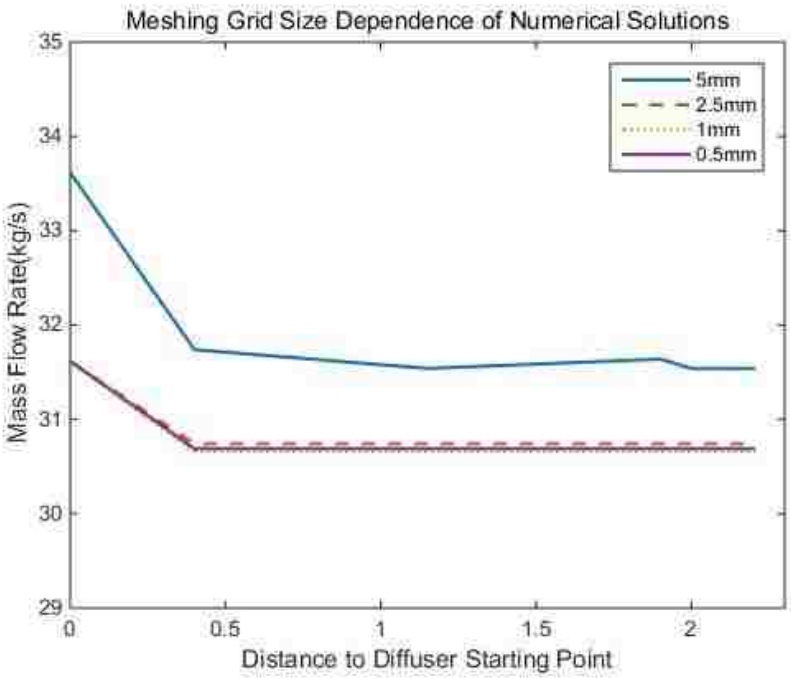


(a)

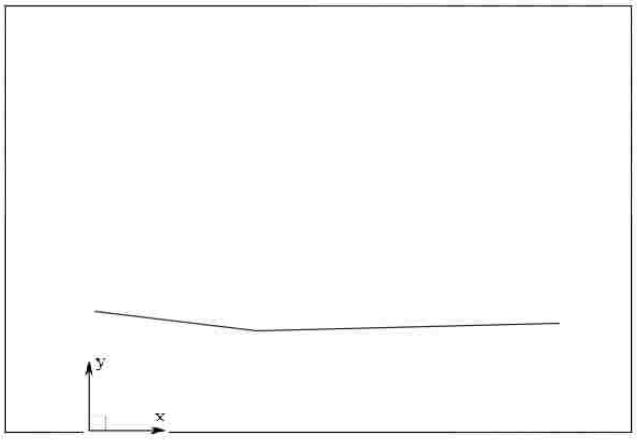


(b)

Figure 3.7: (a) shows Mass flow rate at various locations of perforated diffusers, different refinement of mesh around diffusers are compared to determine dependent of mesh size and results. (b) shows location of diffuser starting point and direction of x axis used in (a).

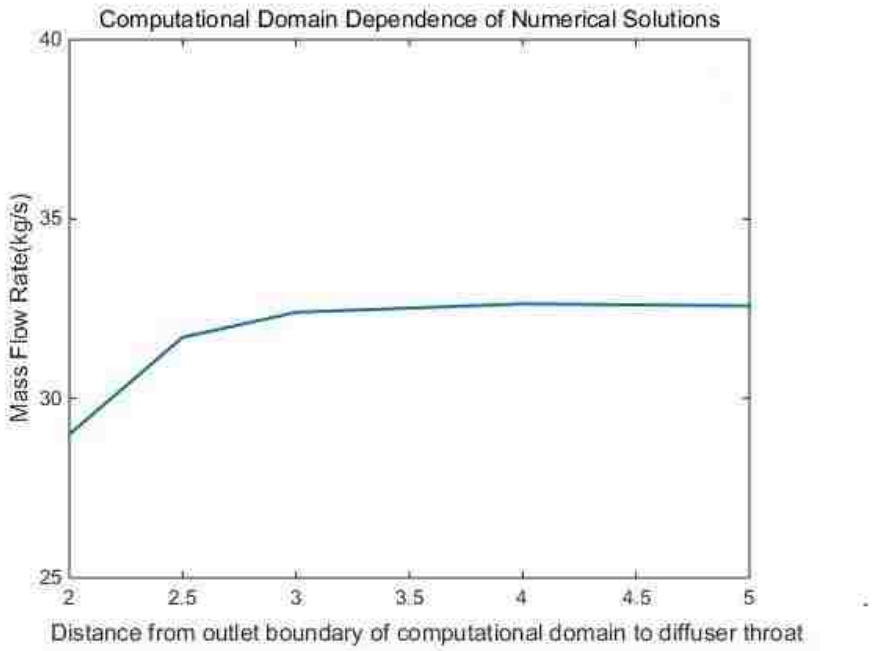


(a)

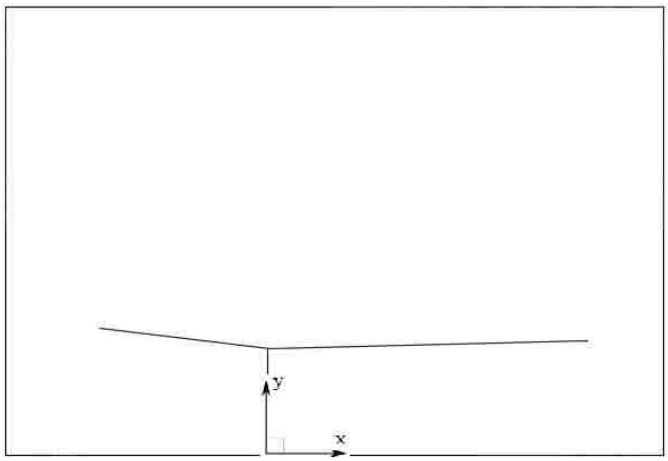


(b)

Figure 3.8: Mass flow rate at the outlet of perforated diffuser vs distance from outlet boundary of computational domain to diffuser throat. (b) shows location of diffuser throat and direction of x axis used in (a).

# Chapter 4

# Results

## 4.1 Validation Simulations

An oblique shock can be formed when a supersonic flow over a concave corner[26]. The relationship among the deflection angle, the shock wave angle, and Mach number (theta-beta-Mach relation) can be expressed as:

$$tan\theta = 2cot\beta \left[ \frac{M_1^2 sin^2\beta - 1}{M_1^2 \left(\gamma + cos2\beta\right) + 2} \right] \tag{4.1}$$

For a given deflection angle, the oblique shock wave angle can be calculated based on an analytical solution to the theta-beta-Mach relation given in the reference[27]:

$$tan\beta = \frac{b + 9atan\mu}{2(1 - 3ab)} - \frac{d(27a^2 tan\mu + 9ab - 2}{6a(1 - 3ab)} \times tan \left[ \frac{n}{3}\pi + \frac{1}{3} arctan\frac{1}{d} \right] \tag{4.2}$$

Where $n$ can be 0,1 corresponding to the weak shock solution, strong shock solution. In equation above, $u$ is Mach wave angle, and

$$a = \left( \frac{\gamma - 1}{2} + \frac{\gamma + 1}{2} tan^2\mu \right) tan\theta$$

$$b = \left( (\frac{\gamma + 1}{2} + \frac{\gamma + 3}{2} tan^2\mu \right) tan\theta$$

$$d = \sqrt{\frac{4(1-3ab)^3}{(27a^2c+9ab-2)^2} - 1}$$

For the supersonic flow over the 23-degree wedge at Mach number 1.5, no real positive solution for the shock wave angle can be determined since the deflection angle is larger than the maximum deflection angle. At this condition, solutions do not exist for the formation of a straight oblique shock instead a curved, detached bow wave will be formed at the upstream as sketched in Figure 4.1 (b). However, for flow over 2.86-degree wedge at Mach number 1.6, a real solution exists, as a result, a straight, attached oblique shock with 48-degree shock wave angle is expected to be formed, as shown in Figure 4.1(a).

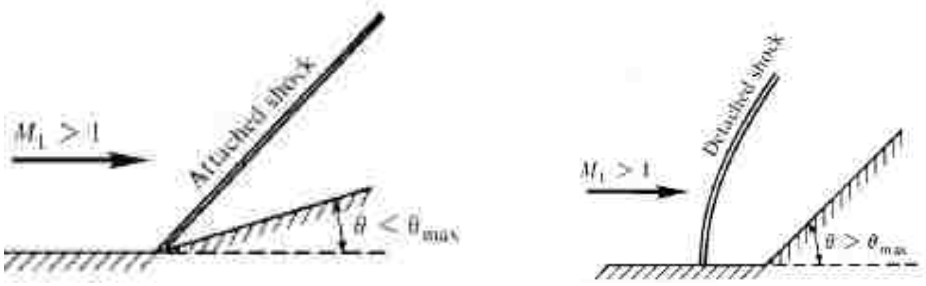


(a) Attached shock (b) Detached shock

Figure 4.1: Attached oblique shock (a) and Detached shock (b)

### 4.1.1 23 Degree Wedge

Figure (4.2) below are contour plots showing the steady state solution achieved by *rhoCentralFoam* and *sonicFoam*. Its clear that no oblique shock is found in 23-degree wedge geometry, but a steady curved bow shock is captured the upstream of the corner.

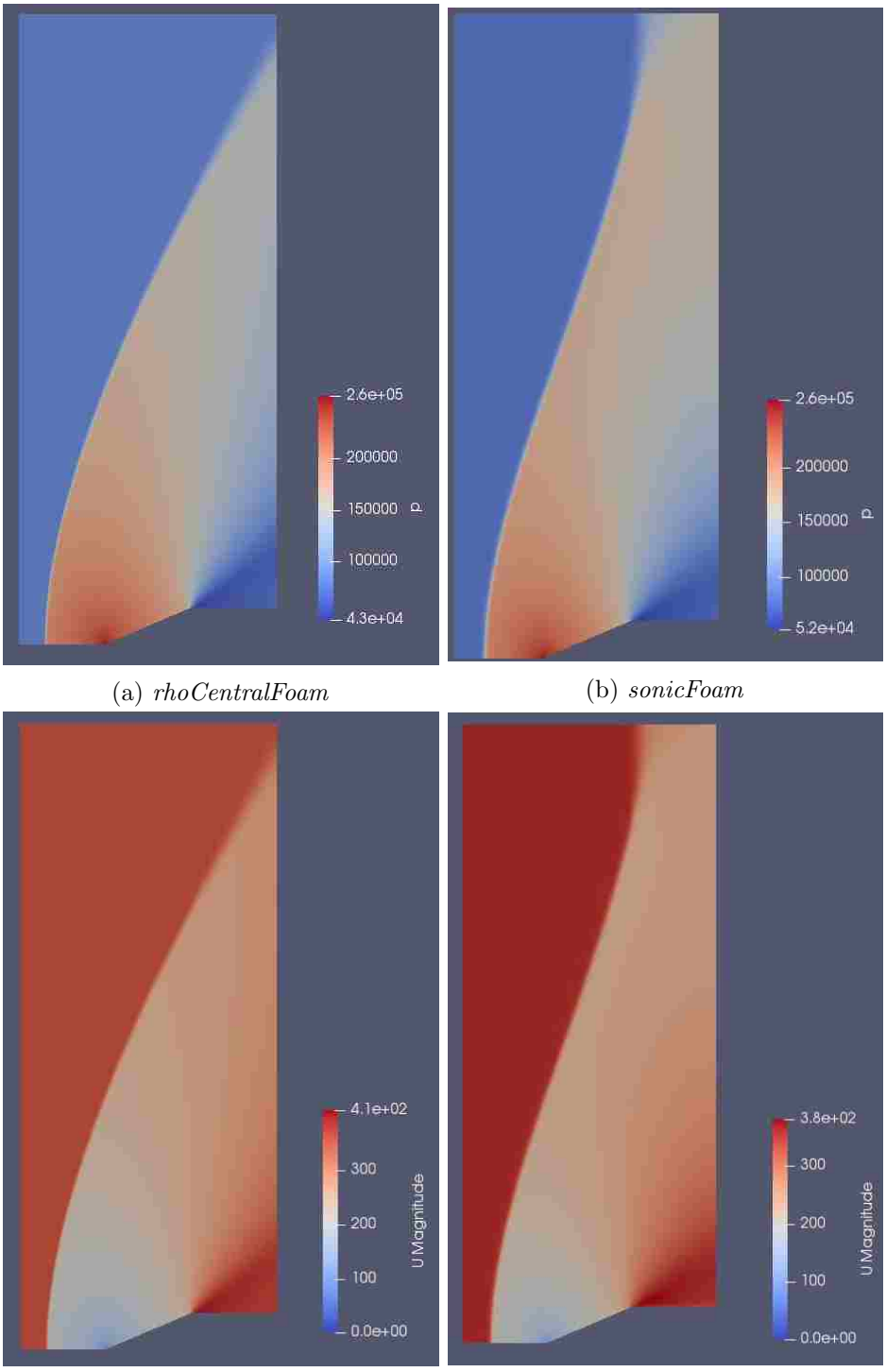


(a) *rhoCentralFoam* (b) *sonicFoam*

(c) *rhoCentralFoam* (d) *sonicFoam*

Figure 4.2: M=1.5 flow over 23 degree wedge. Subfigure (a) shows pressure distribution performed by *r*hoCentralFoam, (b) pressure distribution performed by *s*onicFoam, (c) shows velocity distribution performed by *r*hoCentralFoam and (d) velocity distribution performed by *s*onicFoam

At the centerline, the bow shock is a normal shock. Thus, the centerline pressure ratio can be compared to the normal shock equations:

$$\frac{p_2}{p_1} = 1 + \frac{2\gamma}{\gamma + 1}\left(M_{n1}^2 - 1\right) \tag{4.3}$$

Where $M_{n1}$ is the Mach number at upstream of shock.

From the normal shock equations (4.3), if M1=1.5, p2/p1 across the shock should be 2.82. Using the data for the center-line pressure distribution predicted by the simulation p2/p1 is 2.817 when the *rhoCentralFoam* solver is utilized, and 2.825 when the *sonicFoam* is utilized. Pressures are determined at the first node after the shock. The deviation in predicting pressure jump across the shock is approximately 0.11% for the *rhoCentralFoam* solver and 0.17% for the *sonicFoam* solver.

Comparing result obtained by the sonicFoam and *rhoCentralFoam*, the location of the shock is nearly the same. However, the shock is diffused further away from the wedge, where the mesh is coarse especially for *sonicFoam*. Comparing these results, the profile of the shock obtained from these solvers the shock obtained by *rhoCentralFoam* seems to be sharper and agree well with prediction from theoretical analysis above.

### 4.1.2 2.86 Degree Wedge

For supersonic flow over 2.86-degree wedge, results obtained by the *sonicFoam* and *rhoCentralFoam* solvers are very similar, as shown in Figure 4.3. It is clear that the attached, straight oblique shock is attached to the leading edge of the wedge, and the shock angle is determined to be about 50 degree by inspection. From the oblique shock equations, if M1=1.6, p2/p1 across the shock should be 1.152. From the data of pressure distribution, simulations predict p2/p1 of 1.1522 with the *rhoCentralFoam* solver and 1.1515 with *sonicFoam* solver as calculated at the first node after the shock. The error of predicting pressure jump across the shock is approximately 0.017% with the *rhoCentralFoam* solver and 0.04% with the *sonicFoam* solver.

The mesh of the 2.86-degree wedge geometry is better than the mesh of 23-degree

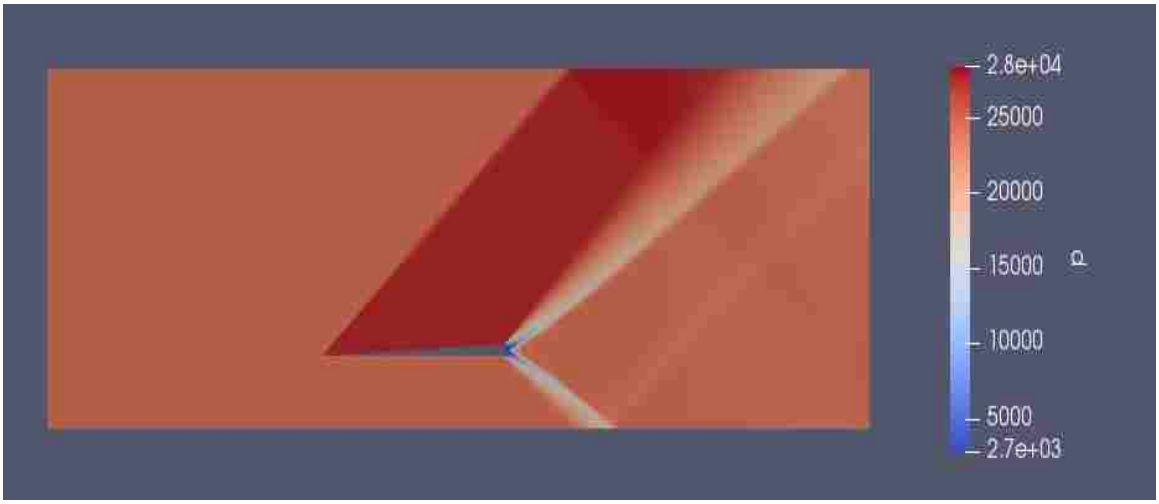


(a) Pressure Distribution(*rhoCentralFoam*)

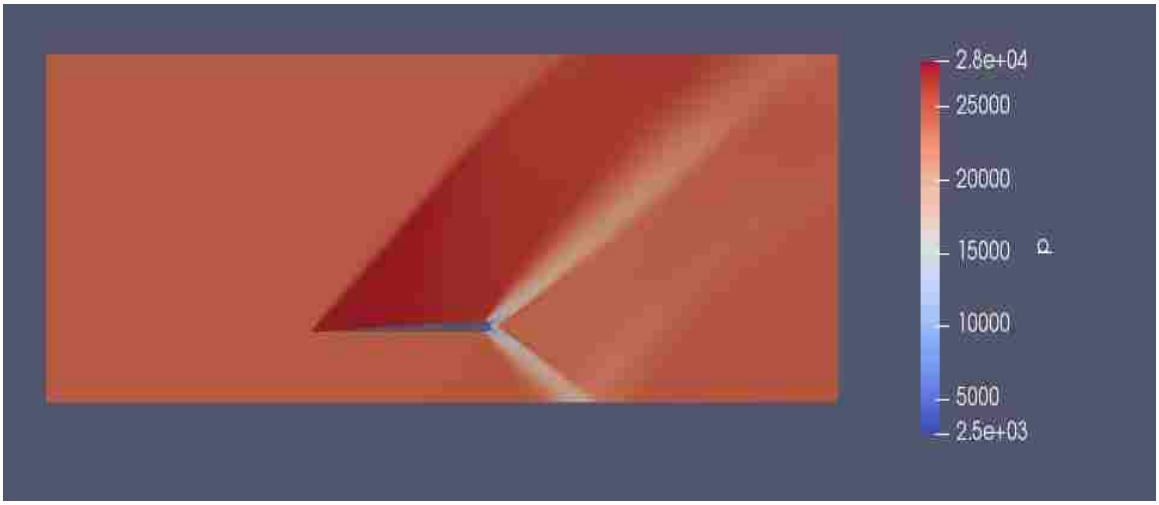


(b) Pressure Distribution(*sonicFoam*)

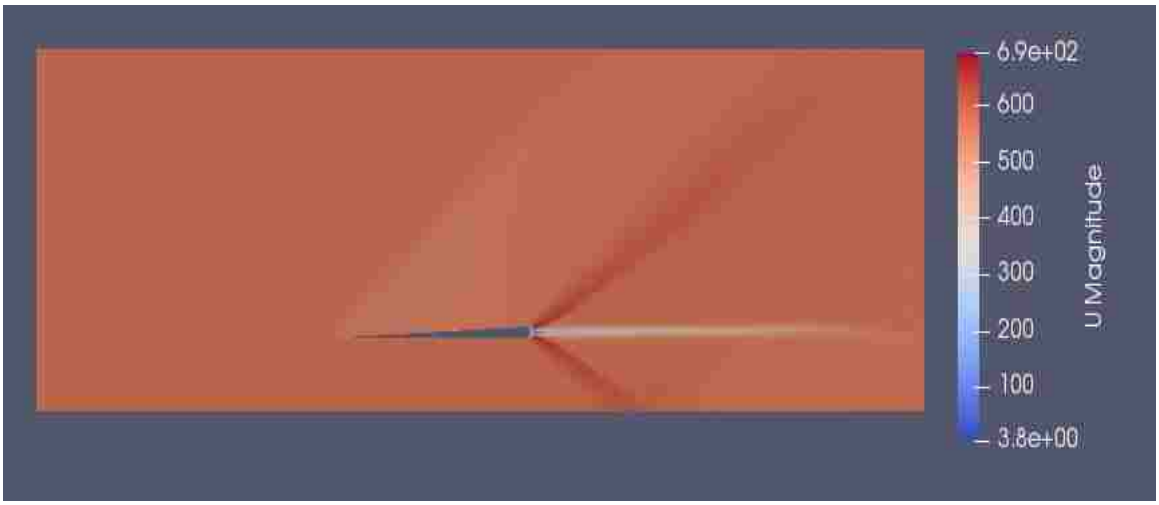


(c) Velocity Distribution(*rhoCentralFoam*)

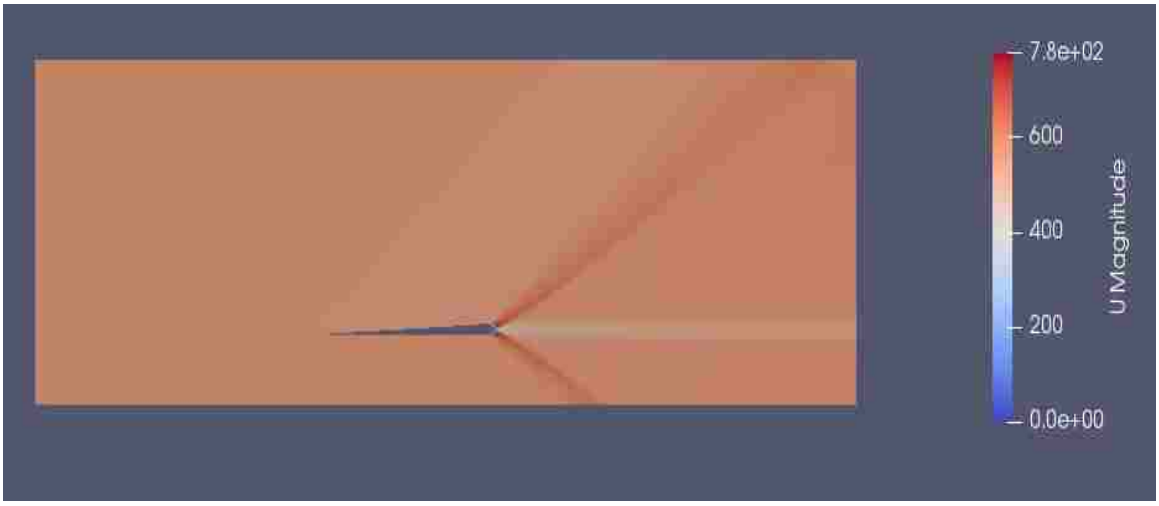


(d) Velocity Distribution(*sonicFoam*)

Figure 4.3: M=1.6 flow over 2.86-degree wedge. (a) is contour of pressure distribution performed by *rhoCentralFoam*, (b) is contour of pressure distribution performed by *sonicFoam*, (c) is contour of velocity distribution performed by *rhoCentralFoam*, (d) is contour of velocity distribution performed by *sonicFoam*

wedge geometry. As a result, the deviation between results obtained by the *sonicFoam* and *rhoCentralFoam* solver is very small, as shown in Figure 4.3. Diffusion of the shock wave is significantly less in the 2.86-degree geometry.

Results above illustrate that the *rhoCentralFoam* and *sonicFoam* can accurately capture the characteristics of the shock wave in compressible supersonic flows. However, the *rhoCentralFoam* performs better when the mesh quality is relatively lower[28].

## 4.2 Diffusers

Figure 4.4 and 4.5 show the pressure and velocity field for supersonic incoming flows over the non-perforated and perforated diffuser at Mach number varying from 1.2 to 2. Flow images displayed in Figure 4.4 and 4.5 are obtained by utilizing the *rhoCentralFoam* solver. Flow images acquired using the *sonicFoam* solver are given in Appendix A.

In the non-perforated nozzle geometry, the flow is choked at the minimum area, and a bow shock is formed. The position of the bow shock is closer to the diffuser as Mach number is increased. In the perforated nozzle geometry, some fluid is bleeding through perforations in the convergent section of the nozzle. While the bow shock is still obvious, the bow shock moves downstream as compared to the same incoming flow in the nonperforated nozzle geometry. Particularly, the engine can swallow the bow shock in the diffuser at the incoming free stream flow velocity larger than Mach 1.8.

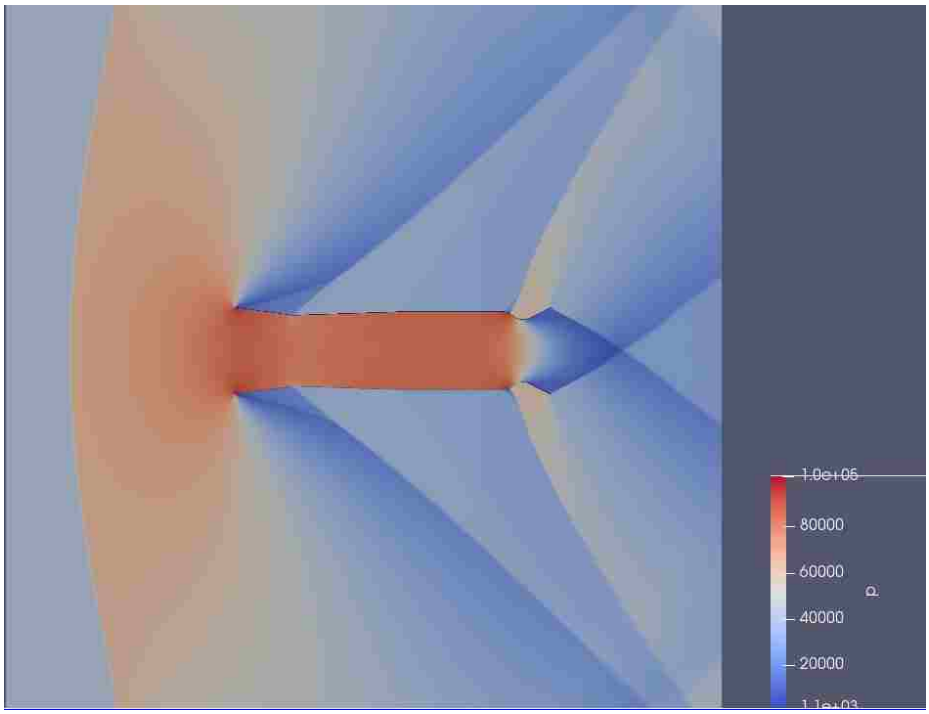


(a) M=1.2(Non-Perforated)

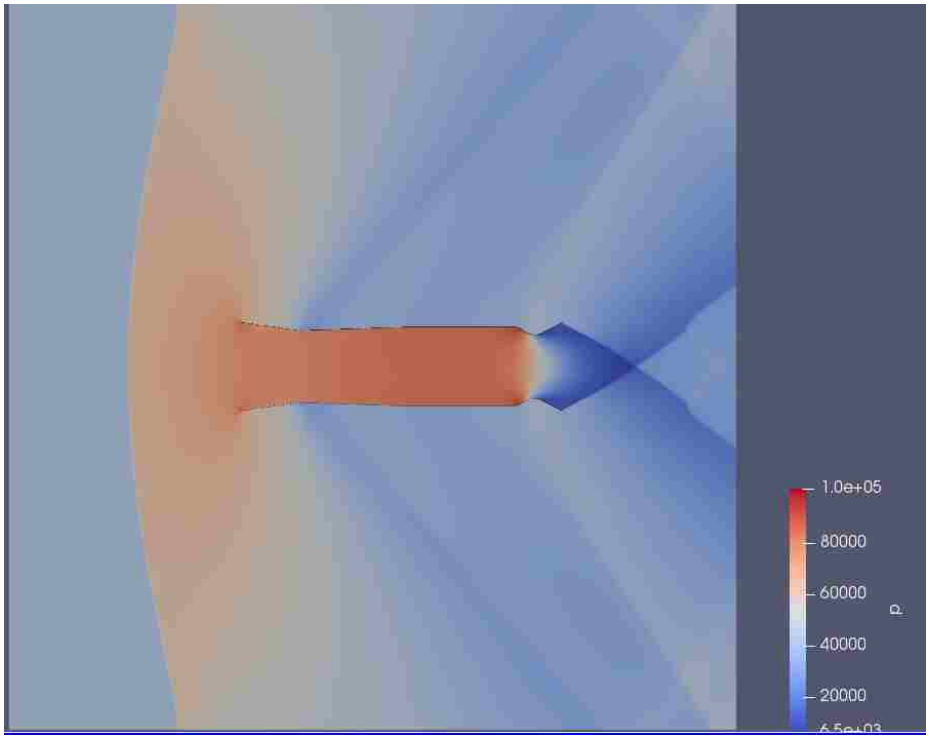


(b) M=1.2(Perforated)

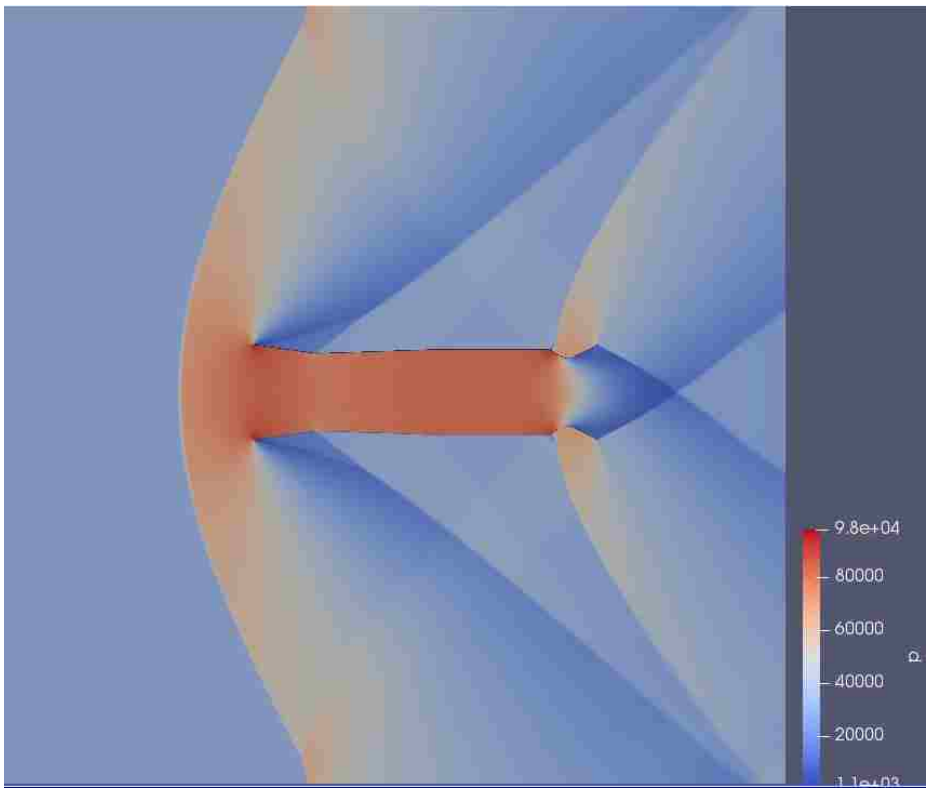


(c) M=1.4(Non-Perforated)

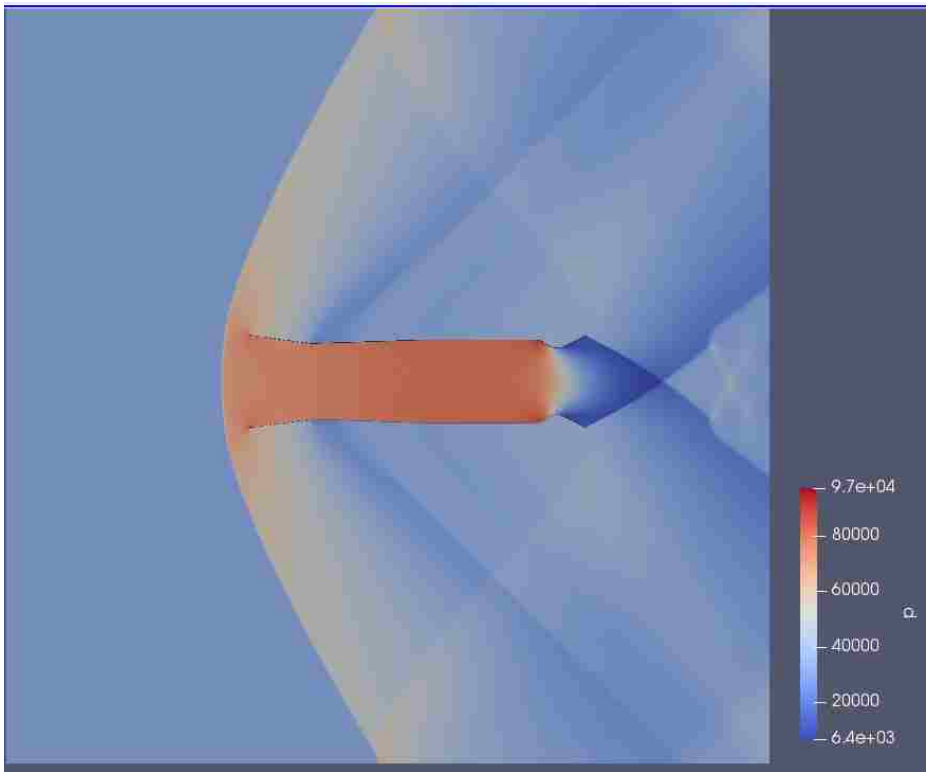


(d) M=1.4(Perforated)

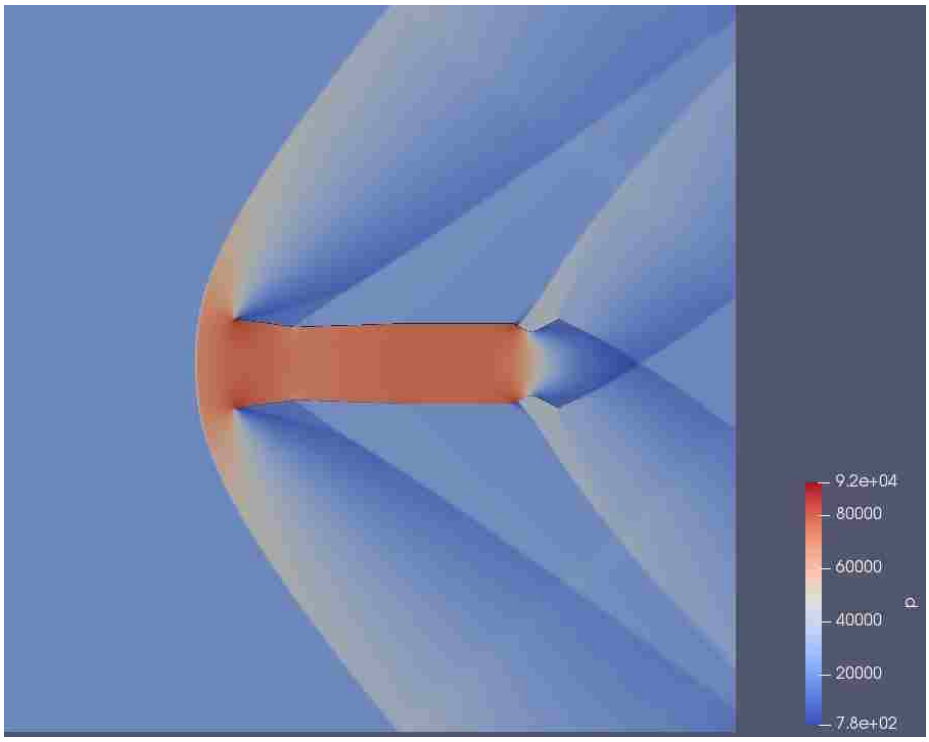


(e) M=1.6(Non-Perforated)

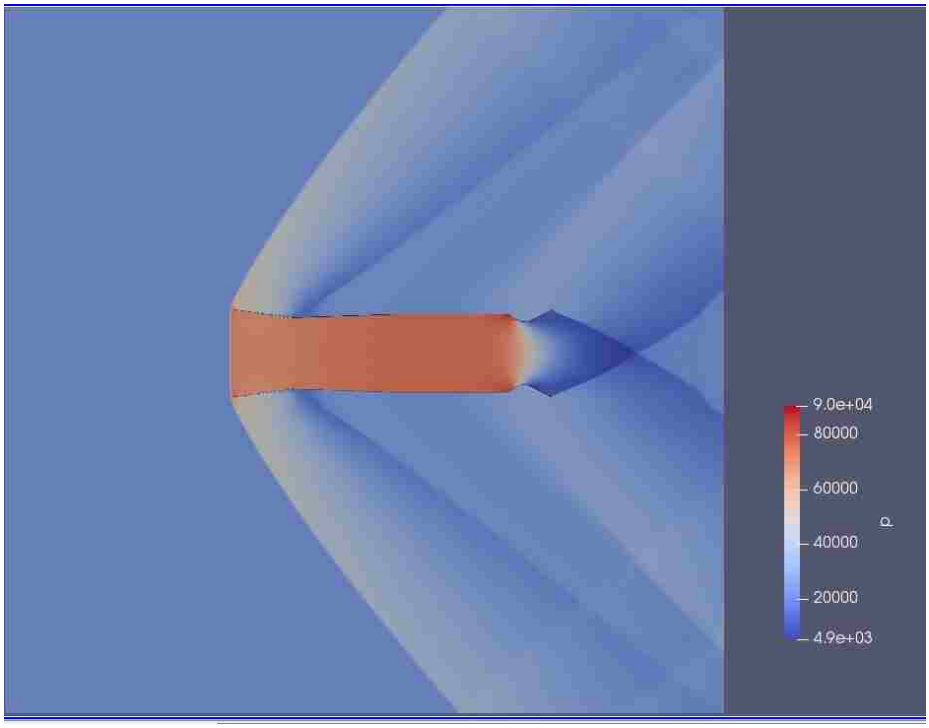


(f) M=1.6(Perforated)

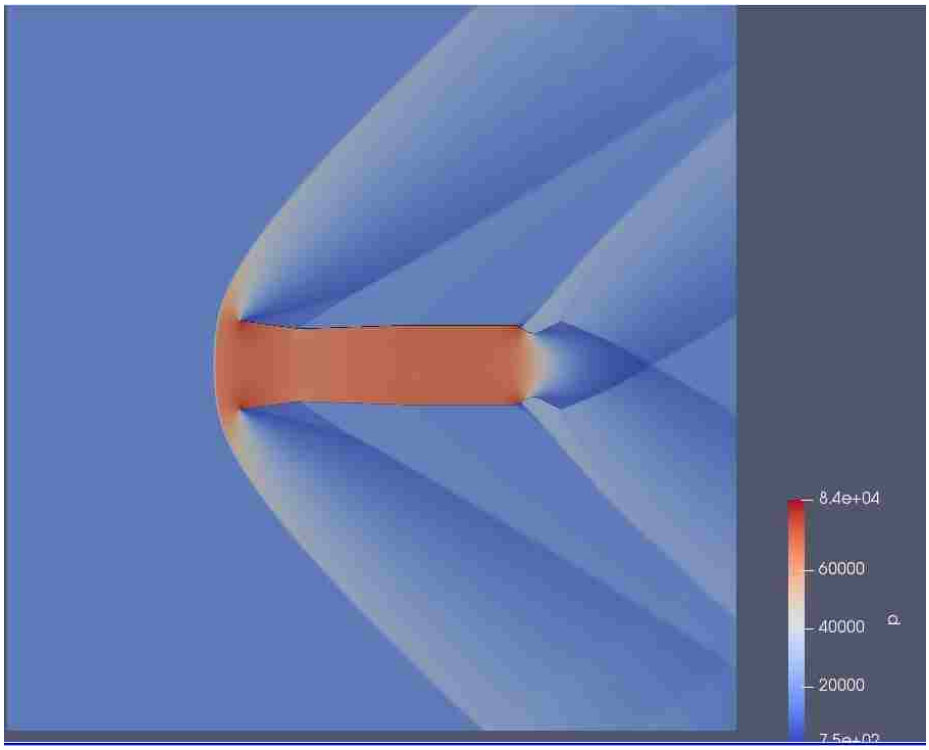


(g) M=1.8(Non-Perforated)

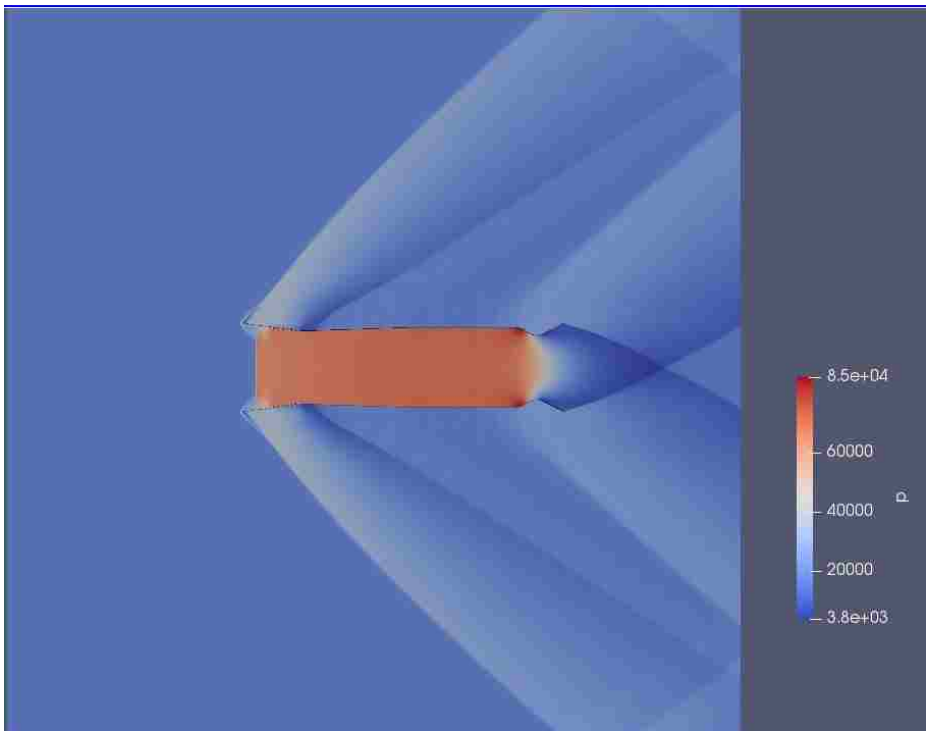


(h) M=1.8(Perforated)

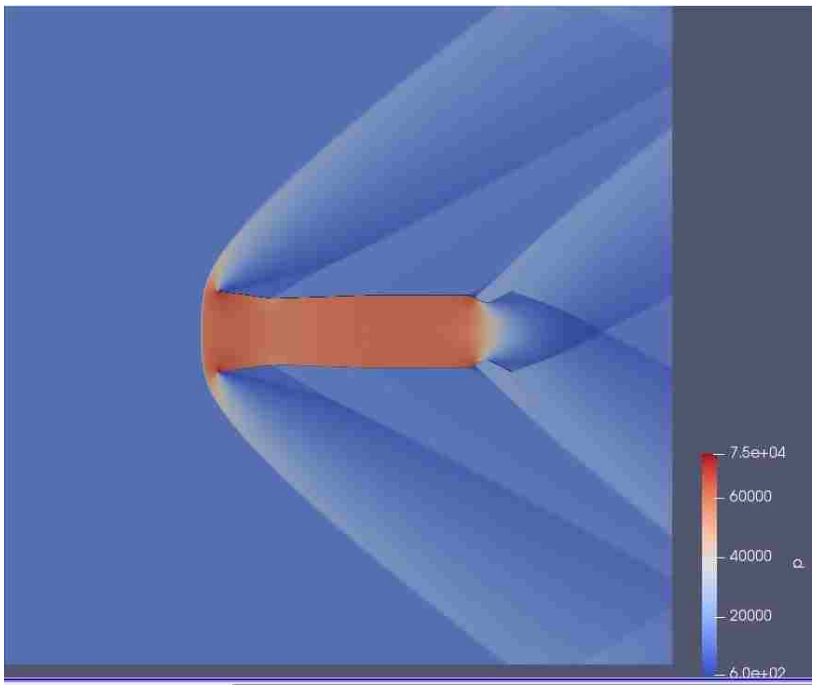


(i) M=2.0(Non-Perforated)

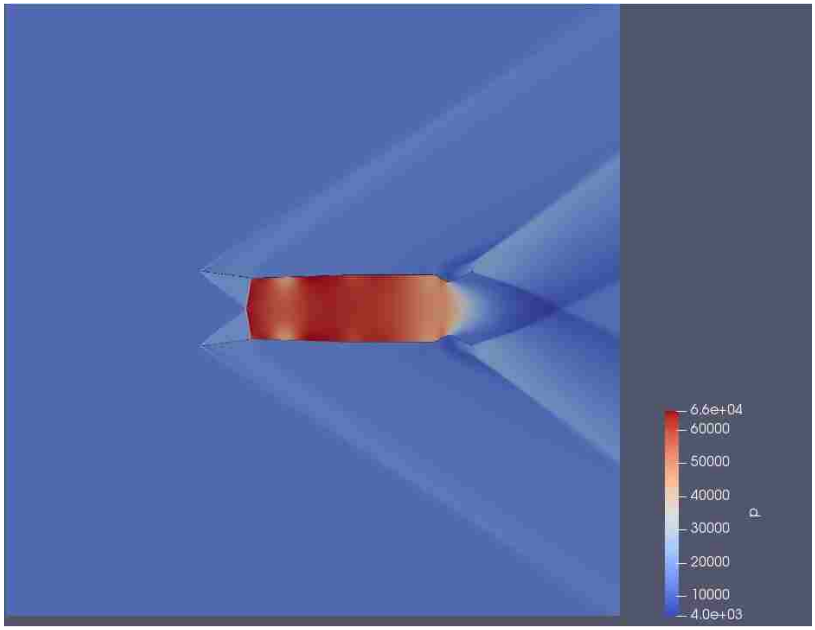


(j) M=2.0(Perforated)

Figure 4.4: Contours of Pressure Distribution of Supersonic Flow Over Diffuser for incoming supersonic flow from (a) Mach=1.2 for non-perforated diffuser, (b) Mach=1.2 for perforated diffuser, (c)Mach=1.4 for non-perforated diffuser ,(d)Mach=1.4 for perforated diffuser, (e) Mach=1.6 for non-perforated diffuser,(f) Mach=1.6 for perforated diffuser, (g) Mach=1.8 for non-perforated diffuser, (h)Mach=1.8 for perforated diffuser, (i) Mach=2.0 for non-perforated diffuser and (j)Mach=2.0 for non-perforated diffuser.

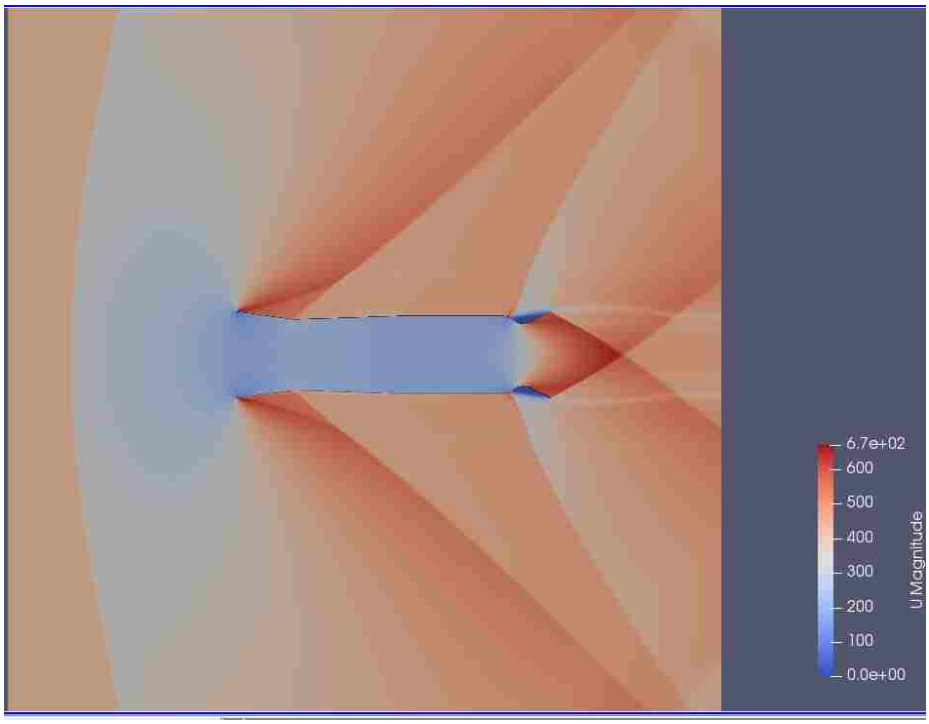


(a) M=1.2(Non-Perforated)

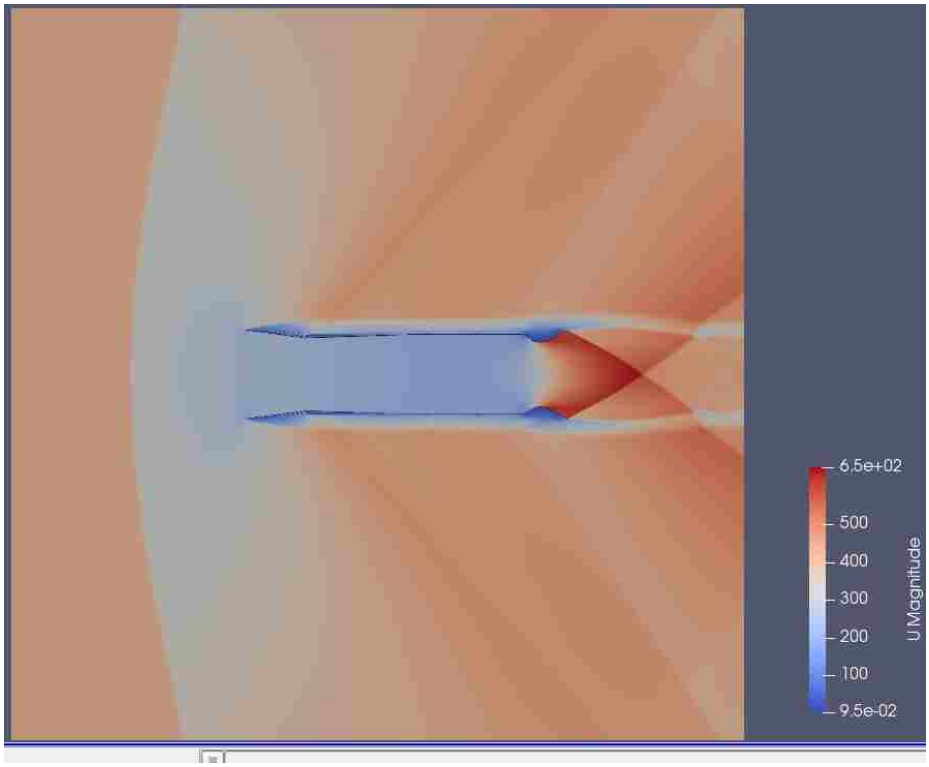


(b) M=1.2(Perforated)

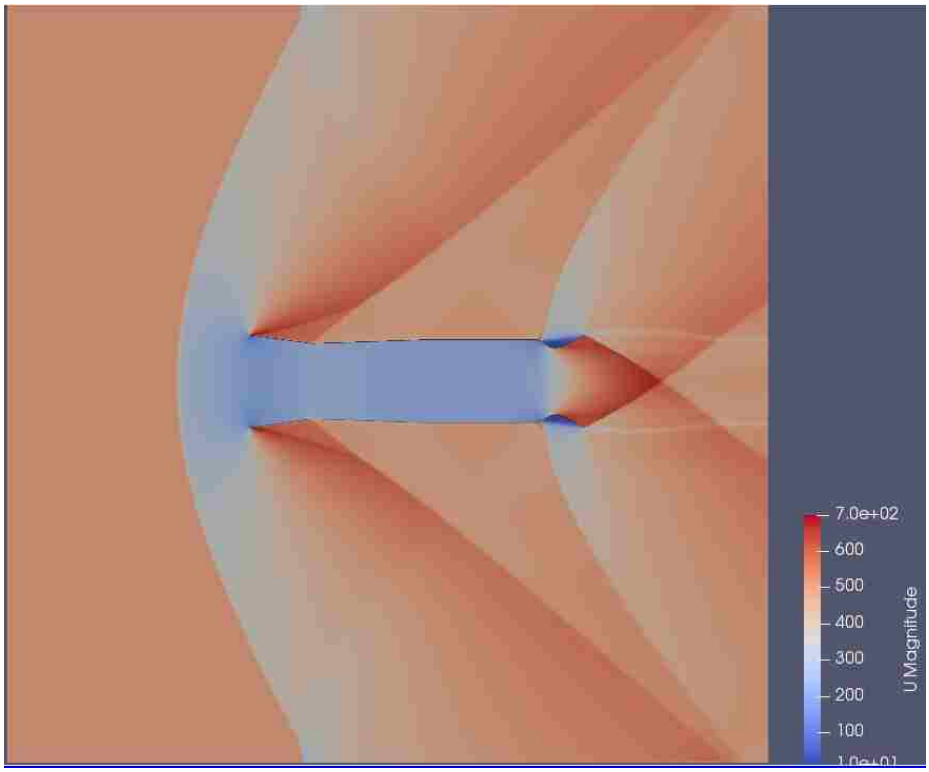


(c) M=1.4(Non-Perforated)

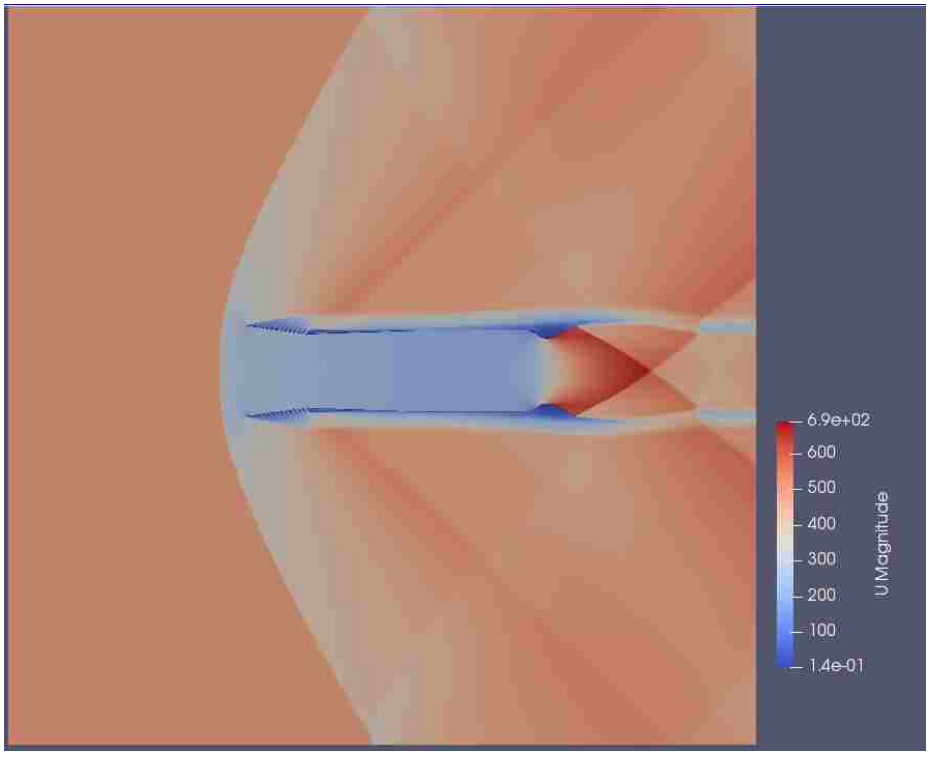


(d) M=1.4(Perforated)

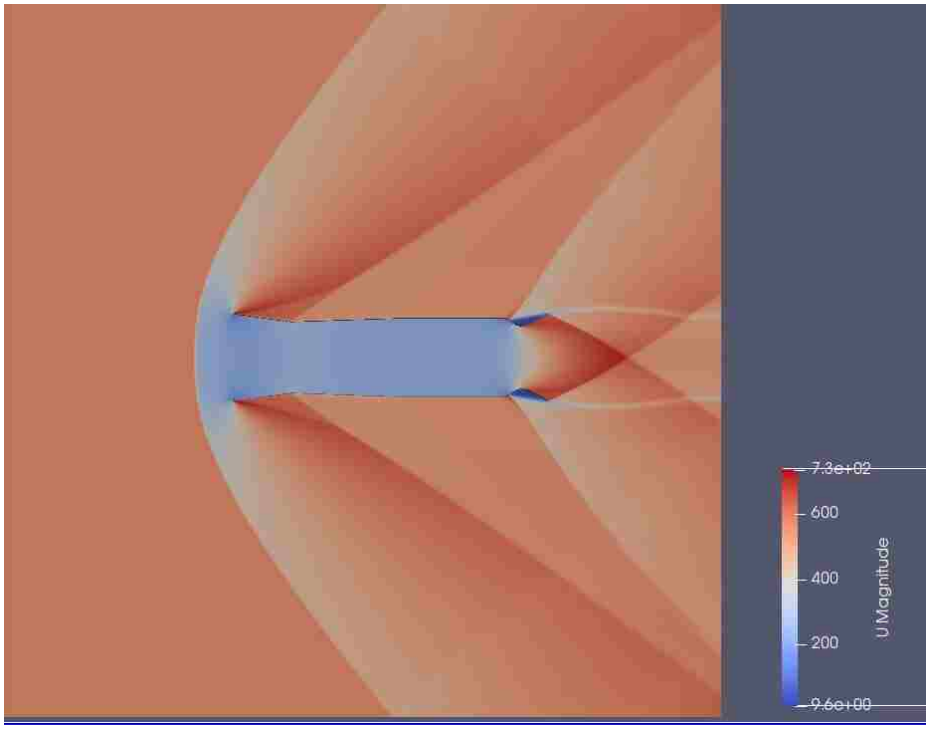


(e) M=1.6(Non-Perforated)

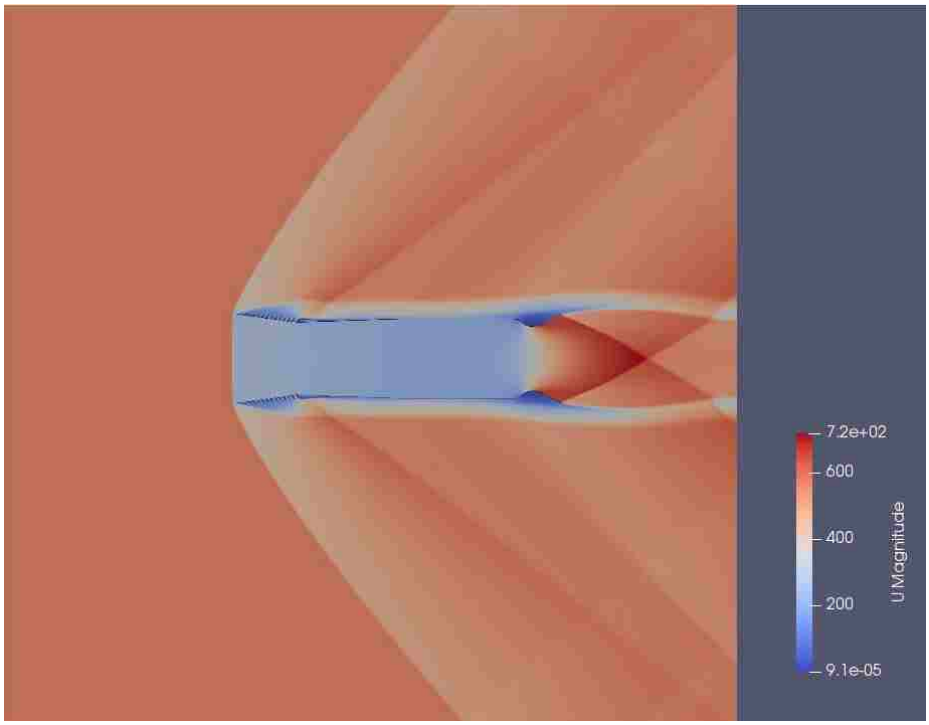


(f) M=1.6(Perforated)

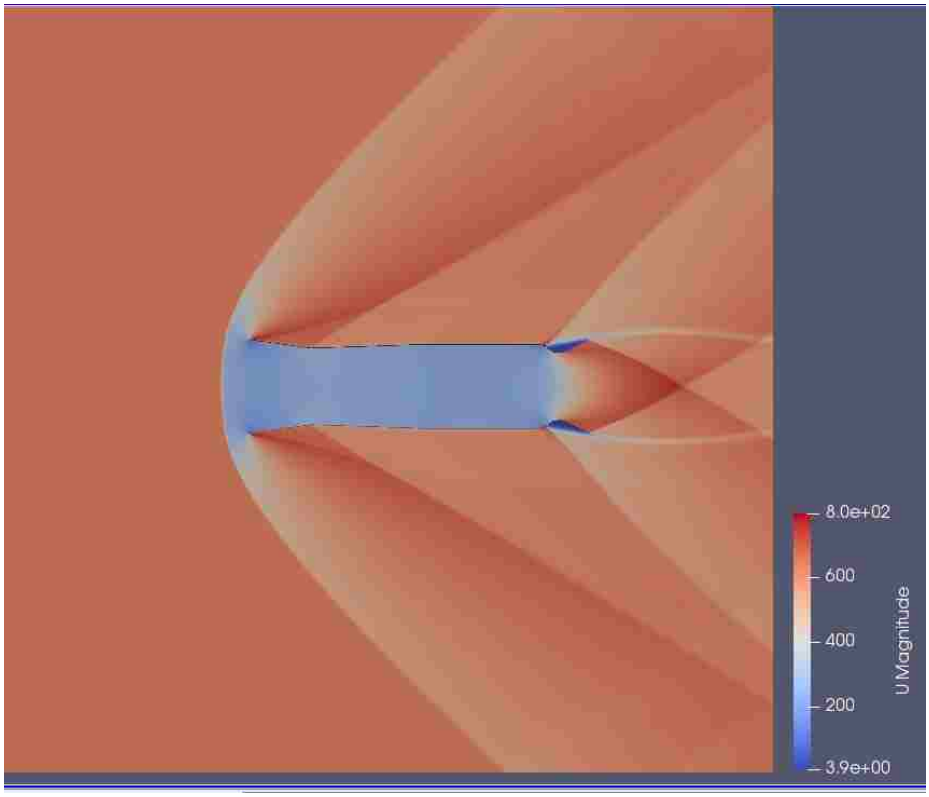


(g) M=1.8(Non-Perforated)

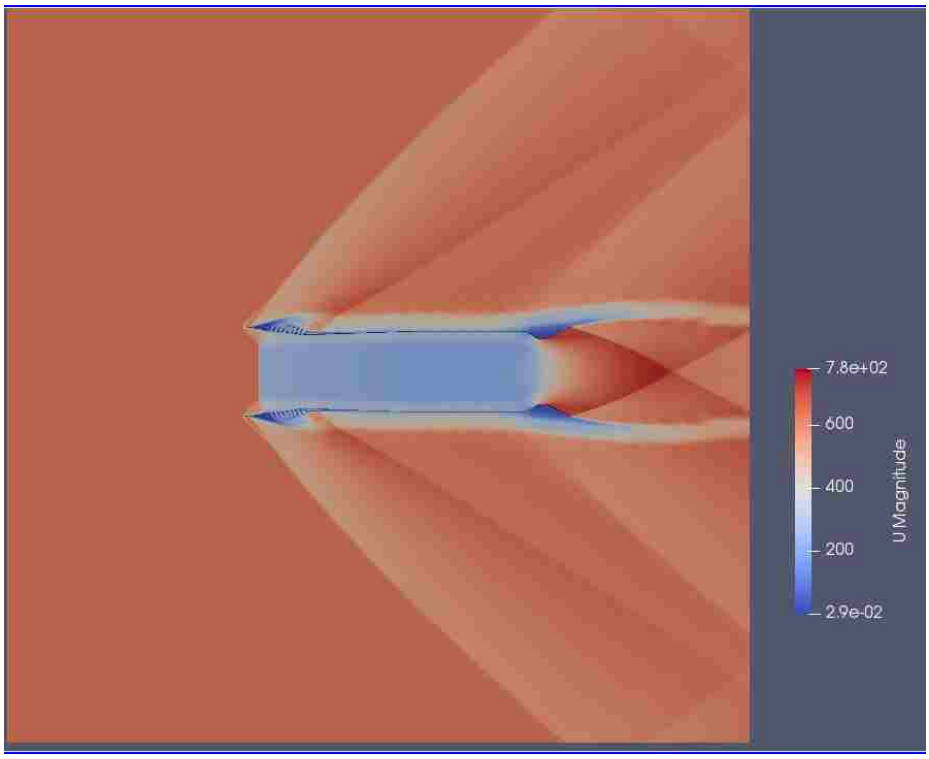


(h) M=1.8(Perforated)

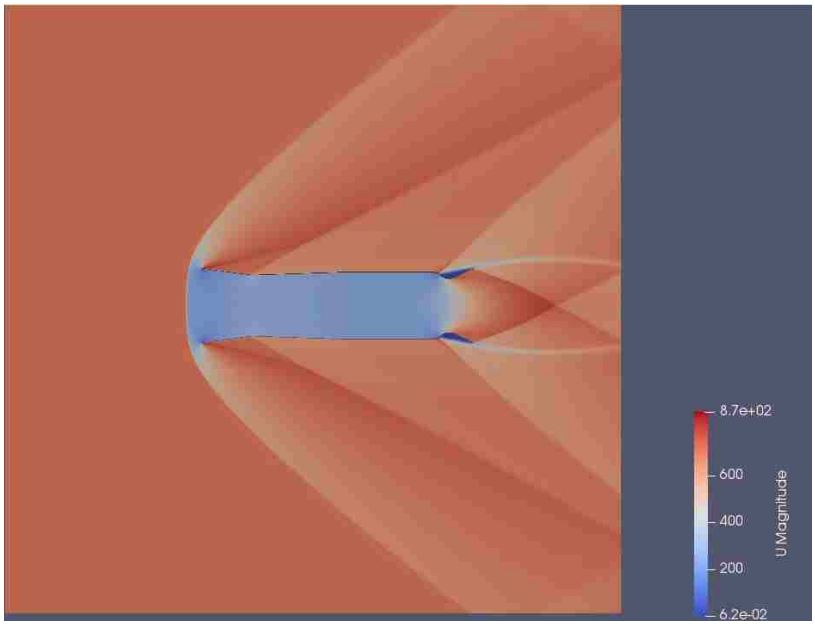


(i) M=2.0(Non-Perforated)

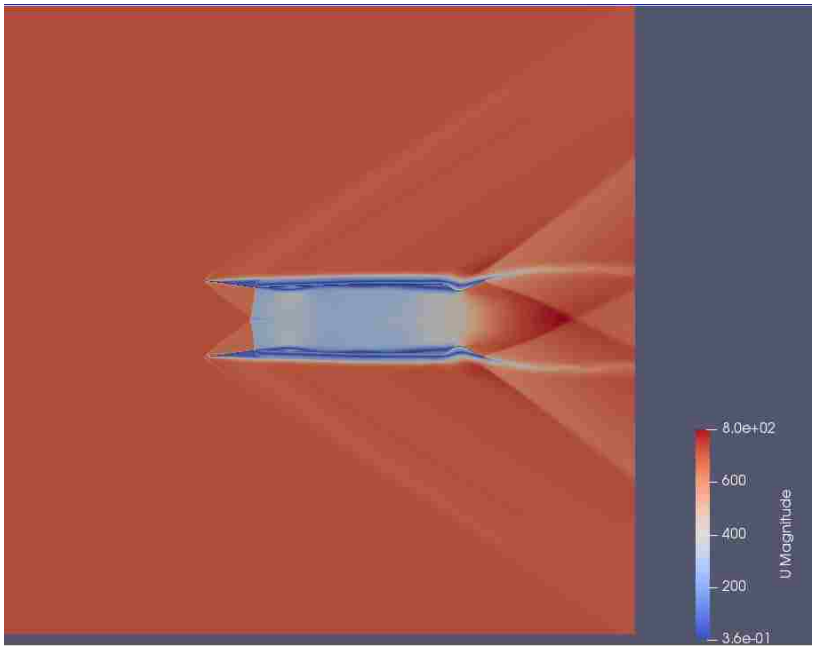


(j) M=2.0(Perforated)

Figure 4.5: Contours of velocity Distribution of Supersonic Flow Over Diffuser for incoming supersonic flow from (a) Mach=1.2 for non-perforated diffuser, (b) Mach=1.2 for perforated diffuser, (c)Mach=1.4 for non-perforated diffuser ,(d)Mach=1.4 for perforated diffuser, (e) Mach=1.6 for non-perforated diffuser,(f) Mach=1.6 for perforated diffuser, (g) Mach=1.8 for non-perforated diffuser, (h)Mach=1.8 for perforated diffuser, (i) Mach=2.0 for non-perforated diffuser and (j)Mach=2.0 for non-perforated diffuser.

### 4.2.1 Location of Shocks

The profiles of the static pressure along the centerline between the inlet of the computational domain and the diffuser are depicted in Figure 4.6 for Mach number 1.6, 1.8 and 2.0. The location of the shock can be determined from the profiles easily as the pressure jumps across the shock wave. In Figure 4.6, the discontinuous change of the static pressure reveals the location of the bow shock. Table 4.1 lists the precise location of the bow shock for different values of Mach number in both diffuser geometry  perforated and nonperfortaed. Results above illustrate the function of perforations discussed in chapter one.

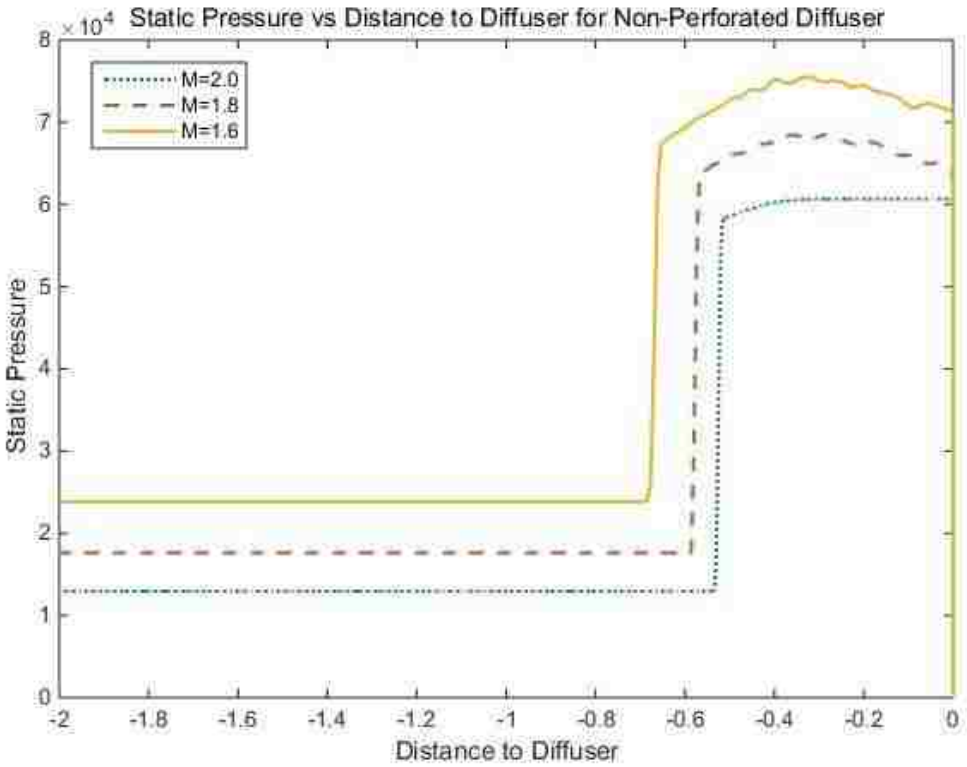


Figure 4.6: Centerline Static Pressure for Non-Perforated Diffuser

| Mach Number | M=1.2 | M=1.4 | M=1.6 | M=1.8 | M=2.0 |
|---|---|---|---|---|---|
| Non-Perforated Diffuser/X(m) | 1.57 | 0.894 | 0.684 | 0.584 | 0.534 |
| Perforated Diffuser/X(m) | 1.198 | 0.592 | 0.438 | 0.31(in) | 0.104(in) |

*X: Upstream Distance to Difffuser Throat

*in: Shock is swallowed in Diffuser

Table 4.1: Location of shocks.

### 4.2.2 Total pressure recovery ratio

Average static pressure, velocity, and temperature at the diffuser throat are recorded every 0.01s. Using the recorded data we calculate the total pressure by:

$$\frac{p}{p_t} = \left(1 + \frac{\gamma - 1}{2} M^2\right)^{-\frac{\gamma}{\gamma - 1}} \tag{4.4}$$

where,

$$M = \frac{v}{a}$$

$$a = \sqrt{\gamma R T}$$

The total-pressure ratio across the normal shock wave which is calculated by equation[29]:

$$\frac{p_{t1}}{p_{t0}} = \left[\frac{(\gamma + 1)M^2}{(\gamma - 1)M^2 + 2}\right]^{\frac{\gamma}{\gamma - 1}} \left[\frac{\gamma + 1}{2\gamma M^2 - (\gamma - 1)}\right]^{\frac{1}{\gamma - 1}} \tag{4.5}$$

Where $p_{t1}$ is total pressure at downstream of shock wave, $p_{t0}$ is total pressure before shock wave.

The total-pressure recovery ratio across the shock wave in the non-perforated and the perforated diffuser geometry is plotted as a function of the Mach number in Figure 4.7. The total-pressure recovery ratio in the non-perforated diffuser geometry is the same as the total-pressure ratio across the normal shock.

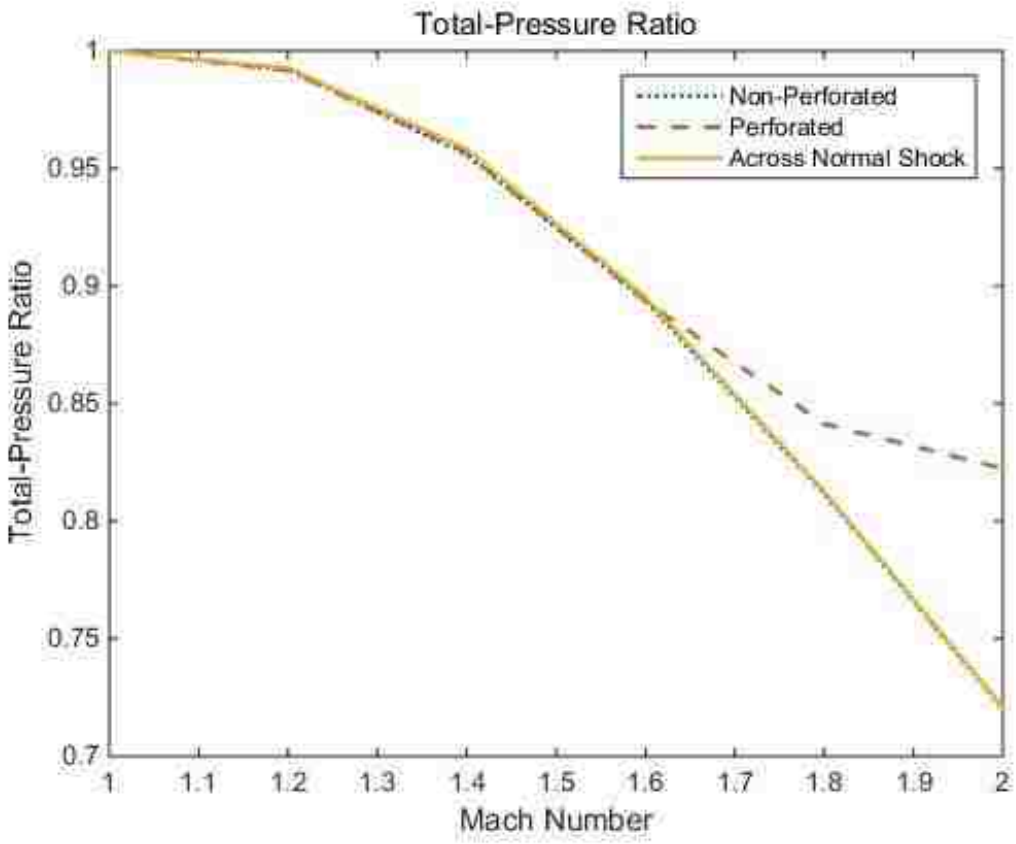


Figure 4.7: Total Pressure Recovery Ratio

In the perforated diffuser geometry, the total-pressure recovery ratio is much greater than that in the non-perforated diffuser geometry when incoming flow Mach number exceeds 1.8. The reason is that from equation 4.5, the total-pressure ratio across the shock will increase as the velocity at the upstream of the shock is decelerated in the convergent section of the nozzle when the shock is swallowed in the diffuser. For example, the total-pressure recovery ratio of the perforated diffuser is 0.82 at Mach number of 2. This value can be compared with the value of 0.72 obtained in the non-perforated diffuser geometry. Thus, the perforated diffuser has demonstrated that the stagnation pressure loss across the bow shock may be eliminated if the shock is swallowed into the diffuser when a sufficient number of holes is drilled.

### 4.2.3 Mass flow rate

The mass flow rate at the entrance and the throat of perforated nozzle is recorded during simulations. Figure 4.8 shows the mass flow rate at perforated inlet and the throat as a function of incoming flow Mach number. At the same time, the leakage of flow through perforations is the difference between the mass flow rate at the entrance and the throat which is calculated and listed in Table 4.2.

As is illustrated in Figure 4.8 and Table 4.2 that when the flow through the convergent section of the nozzle is subsonic, a large amount of mass will bleed through perforations. At Mach number 1.6, nearly 20% of mass will be leaked through holes. However, when the bow shock is swallowed by the diffuser, it is immune to seeping through the perforations because the convergent section of the nozzle is supersonic. As stated in the chapter 1, when a supersonic flow is established in the convergent inlet, low pressure difference will exist across the orifices. At the same time, the orifices become less effective because the high-speed air has less time to swerve and pass through the holes. These factors tend to reduce the loss of mass flow through the perforations as compared with the subsonic regime.

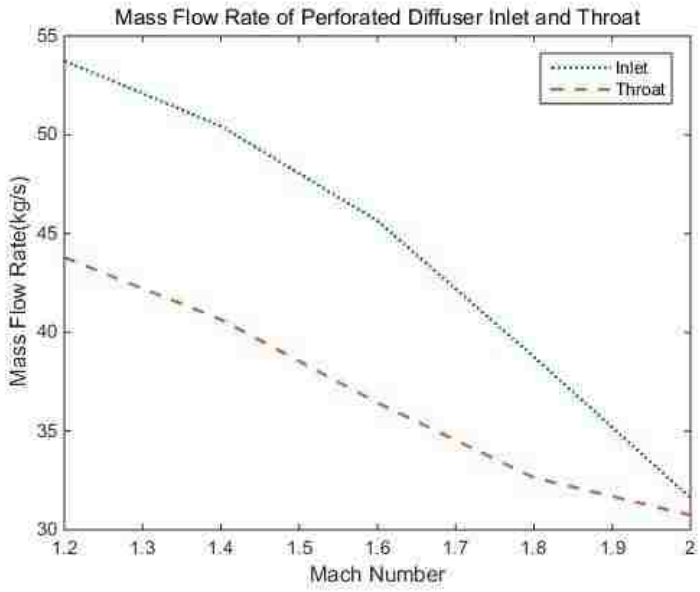


Figure 4.8: Mass Flow Rate at Perforated Diffuser Inlet and Throat vs Mach Number.

| Mach Number | M=1.2 | M=1.4 | M=1.6 | M=1.8 | M=2.0 |
|---|---|---|---|---|---|
| "Leakage"(kg/s) | 9.9495 | 9.7978 | 9.2112 | 6.1106 | 0.8767 |

Table 4.2: Mass Flow Rate Loss Through Perforations.

### 4.2.4 *rhoCentralFoam* vs *sonicFoam*

Results obtained by the *sonicFoam* and *rhoCentralFoam* solver are slightly different. When the bow shock is swallowed by the diffuser, the shock predicted by the *rhoCentralFoam* is stationary with a fixed location, but the location of the shock predicted by the for *sonicFoam* solver is oscillating with a well-defined a frequency. The computation time between these two solvers is different as well. The mesh with the diffuser simulations is the same and both satisfy the mesh independency requirement, but the computation time using the *sonicFoam* solver is almost two times greater than that using the *rhoCentralFoam*[28]. Furthermore, a low-speed stream starting at the external wall of the diffuser is observed in non-perforated nozzle geometry when simulating is conducted using the *sonicFoam* solver. This flow characteristic is not expected in inviscid flow within this geometry.

A common flow characteristics is observed by both solvers for flows in the perforated diffuser geometry. The area with extremely low-speed flow will be found outside the perforated convergent section. The influence of mesh size is excluded because similar phenomenon occurred again when running the same simulation with mesh refined to 0.5mm. One reason for this might be some numerical error occurred when running supersonic simulations in a relatively complex geometry. At the same time, a large pressure difference between the internal and external flow at the perforation intersects with a bow shock wave might generate complicated physical phenomenon like this.

# Chapter 5

# Conclusion

A series of computational fluid dynamics simulations was performed on supersonic flows over perforated and non-perforated diffusers by utilizing OpenFoam. Inviscid simulations are conducted for a range of Mach number from 1.2 to 2.0.

Two compressible solvers *sonicFoam* and *rhoCentralFoam* are used in this study. The SonicFoam, a pressure based solver, uses the PIMPLE method, and the *rhoCentralFoam*, a density based solver, uses an alternative approach to Riemann solvers constructed on the central-upwind schemes.

Simulations are conducted to validate the mathematical model and numerical methods, simulations are conducted. Supersonics flows over 23 degree wedge at Mach number 1.5 and over 2.86 degree wedge at Mach number 1.6 are considered for validation. A straight oblique shock attached to the wedge with nearly 50 degree shock wave angle is observed at Mach number 1.6 for flows over the 2.86 degree wedge. Predicted results agree well with results obtained by the analytical method. The difference in the pressure ratio across the shock predicted by the numerical solution and the analytical solution is less than 1% in each geometry. These results validate the mathematical model and the numerical methods employed here.

Simulations of supersonic flows over the perforated and non-perforated diffuser are performed employing the *sonicFoam* and *rhoCentralFoam* solver. Using the velocity and

pressure field at various Mach number we determine the location and the evolution of the bow shock. It is illustrated here that the perforated nozzle inlet makes the bow shock to be swalled by the diffuser when the incoming flow Mach number exceeds 1.8. The loss of total pressure across the bow shock is reduced significantly when bow shock moves inside the nozzle. At Mach number 2, the total pressure drop is reduced more than 64% in the perforated nozzle geometry compared to that in the non-perforated nozzle geometry.

The difference in the mass flow rate at the cross-section of the diffuser inlet and the throat shows that some fraction of fluid bleeds through perforations, resulting in a lower mass flow rate through the engine core and a lower thrust output subsequently. Our results indicate that the mass flow rate drops about 20% drop through the perforated nozzle geometry at Mach number of 1.6 while the drop in the mass flow rate is only 2% at Mach number 2 and above. When the bow shock is swallowed by the diffuser the mass flow rate reduction will be very small and the resulting power losses will be insignificant.

Results above agree well with of the results of the theoretical analysis conducted in the perforated nozzle (see references [7][8][9]). Our numerical simulations predict the presence of low speed region outside the perforated convergent section. We believe that the presence of this small layer is a result of a large pressure difference at perforation section intersecting with the shock. Numerical error might be occurred in complex geometry simulation too.

Results predicted by the *sonicFoam* and *rhoCentralFoam* solver are slightly different. The shock captured by the rhoCentralFoam solver dissipates in a lesser degree. Also, it is demonstrated here that the *rhoCentralFoam* does not require the high degree of resolution that the *sonicFoam* solver requires. It is clearly shown here that the openFoam can be an effective tool to characterize supersonic flows in complex geometries.

# Bibliography


[1] William H Avery. Twenty-five years of ramjet development. *Journal of Jet Propulsion*, 25(11):604–614, 1955.

[2] Robert Winston McCloy. *The fundamentals of supersonic propulsion.* Boeing Co., Supersonic Propulsion Test Group, 1968.

[3] Arthur Kantrowitz and Coleman DuP Donaldson. Preliminary investigation of supersonic diffusers. 1945.

[4] DeMarquis D Wyatt and Henry R Hunczak. An investigation of convergent-divergent diffusers at mach number 1.85. 1951.

[5] PG Hill and CR Peterson. Aerothermodynamics of inlets, combustors, and nozzles. *Mechanics and Thermodynamics of Propulsion*, pages 217–274, 1992.

[6] Ascher H Shapiro. *The dynamics and thermodynamics of compressible fluid flow.* John Wiley & Sons, 1953.

[7] Rudolf Hermann. *Supersonic inlet diffusers and introduction to internal aerodynamics.* Minneapolis-Honeywell Regulator Co., Aeronautical Division, 1956.

[8] Gordon C Oates. *Aerothermodynamics of gas turbine and rocket propulsion.* Aiaa, 1997.

[9] J Seddon and EL Goldsmith. Intake aerodynamics, aiaa education series, aiaa, 1999.

[10] Råbi Bin Tahir. *Analysis of Shock Dynamics in Supersonic Intakes.* PhD thesis, 2009.

[11] John C Evvard and John W Blakey. The use of perforated inlets for efficient supersonic diffusion. 1947.

[12] Henry R Hunczak and Emil J Kremzier. Characteristics of perforated diffusers at free-stream mach number 1.90. Technical report, NATIONAL ADVISORY COMMITTEE FOR AERONAUTICS CLEVELAND OH LEWIS FLIGHT PROPULSION LAB, 1950.

[13] University of Toronto. Institute of Aerophysics. *An Experimental Investigation of a Supersonic Two-dimensional Perforated Inlet at a Nominal Free Stream Mach Number of 2.5*. University of Toronto, Institute of Aerophysics, 1958.

[14] Hongjun Ran and Dimitri Mavris. Preliminary design of a 2d supersonic inlet to maximize total pressure recovery. In *AIAA 5th ATIO and16th Lighter-Than-Air Sys Tech. and Balloon Systems Conferences*, page 7357, 2005.

[15] Rabi Bin Tahir. Starting and unstarting of hypersonic air inlets. *MASc Thesis, Ryerson University*, 2003.

[16] Dongyue Li. icofoam analysis. `http://dyfluid.com/icoFoam.html`.

[17] G Holzinger. Openfoam–a little user-manual, 2015.

[18] Guanyang Xue. *Computational Study of Jet Flows Emanating from a Circular Orifice*. PhD thesis, Lehigh University, 2017.

[19] The OpenFOAM Foundation Ltd. `https://github.com/OpenFOAM/OpenFOAM-dev/tree/master/applications/solvers/compressible/sonicFoam`.

[20] Alexander Kurganov, Sebastian Noelle, and Guergana Petrova. Semidiscrete central-upwind schemes for hyperbolic conservation laws and hamilton–jacobi equations. *SIAM Journal on Scientific Computing*, 23(3):707–740, 2001.

[21] Alexander Kurganov and Eitan Tadmor. New high-resolution central schemes for nonlinear conservation laws and convection–diffusion equations. *Journal of Computational Physics*, 160(1):241–282, 2000.

[22] Christopher J Greenshields, Henry G Weller, Luca Gasparini, and Jason M Reese. Implementation of semi-discrete, non-staggered central schemes in a colocated, polyhedral, finite volume framework, for high-speed viscous flows. *International journal for numerical methods in fluids*, 63(1):1–21, 2010.

[23] The OpenFOAM Foundation Ltd. `https://github.com/OpenFOAM/OpenFOAM-dev/tree/master/applications/solvers/compressible/rhoCentralFoam`.

[24] CURIOSITYFLUIDSADMIN1. `https://curiosityfluids.com/2016/03/28/mach-1-5-flow-over-23-degree-wedge-rhocentralfoam/`.

[25] Trevor Hayes. Perforated nozzle inlets for fixed-geometry ramjets, 2017.

[26] John David Anderson. *Modern compressible flow: with historical perspective*, volume 12. McGraw-Hill New York, 1990.

[27] Lael Voneggers Rudd and Mark J Lewis. Comparison of shock calculation methods. *Journal of aircraft*, 35(4):647–649, 1998.

[28] LF Gutiérrez Marcantoni, JP Tamagno, and SA Elaskar. High speed flow simulation using openfoam. *Mecánica Computacional*, 31:2939–2959, 2012.

[29] National Aeronautics and Space Administration. `https://www.grc.nasa.gov/www/k-12/airplane/normal.html`.

# Appendix A

# Additional Results

Figure A.1 and A.2 show the pressure and velocity field for supersonic incoming flows over the non-perforated and perforated diffuser at Mach number varying from 1.2 to 2. Flow images displayed in Figure A.1 and A.2 are obtained by utilizing the *sonicFoam* solver.

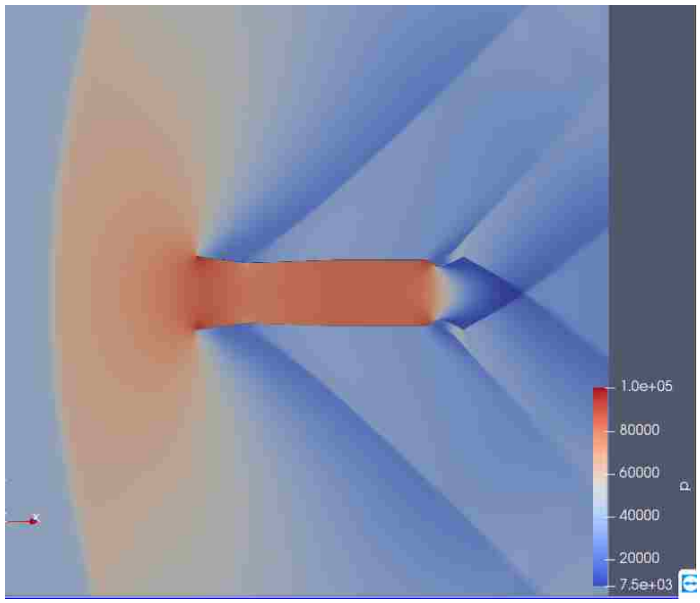


(a) M=1.2(Non-Perforated)

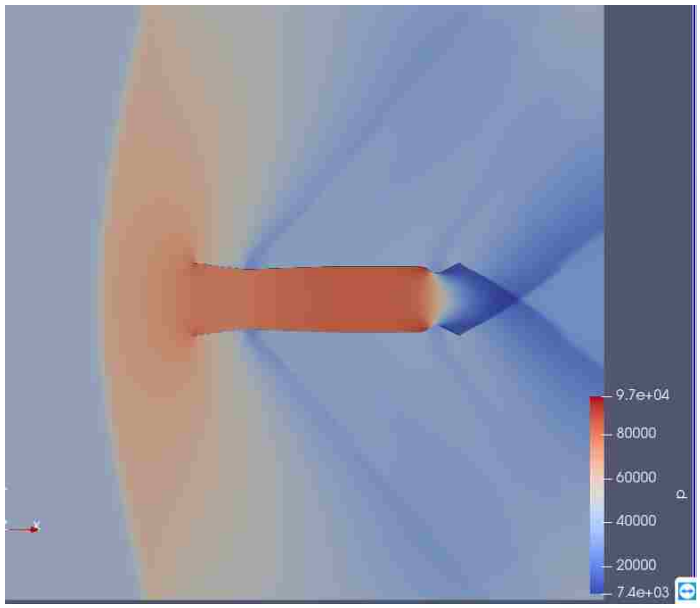


(b) M=1.2(Perforated)

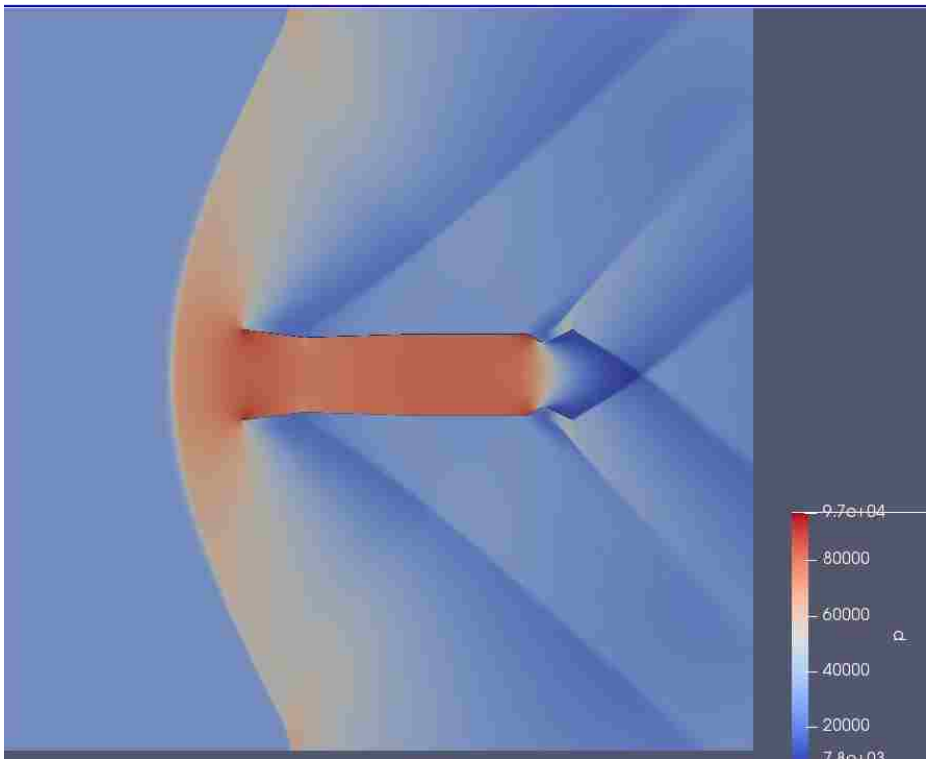


(c) M=1.4(Non-Perforated)

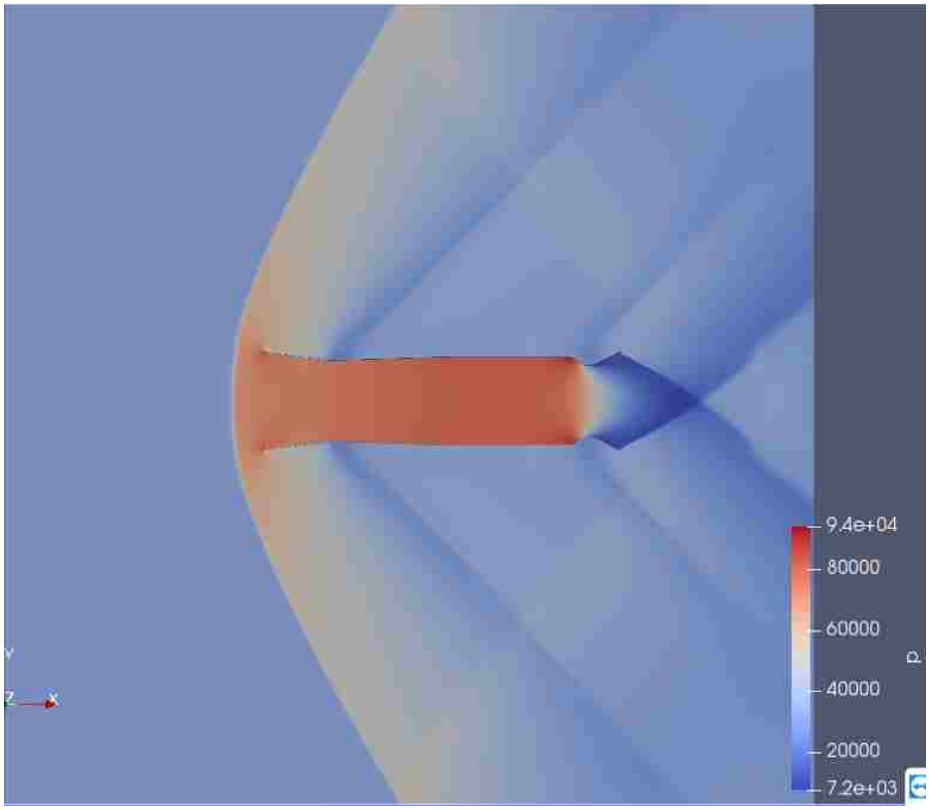


(d) M=1.4(Perforated)

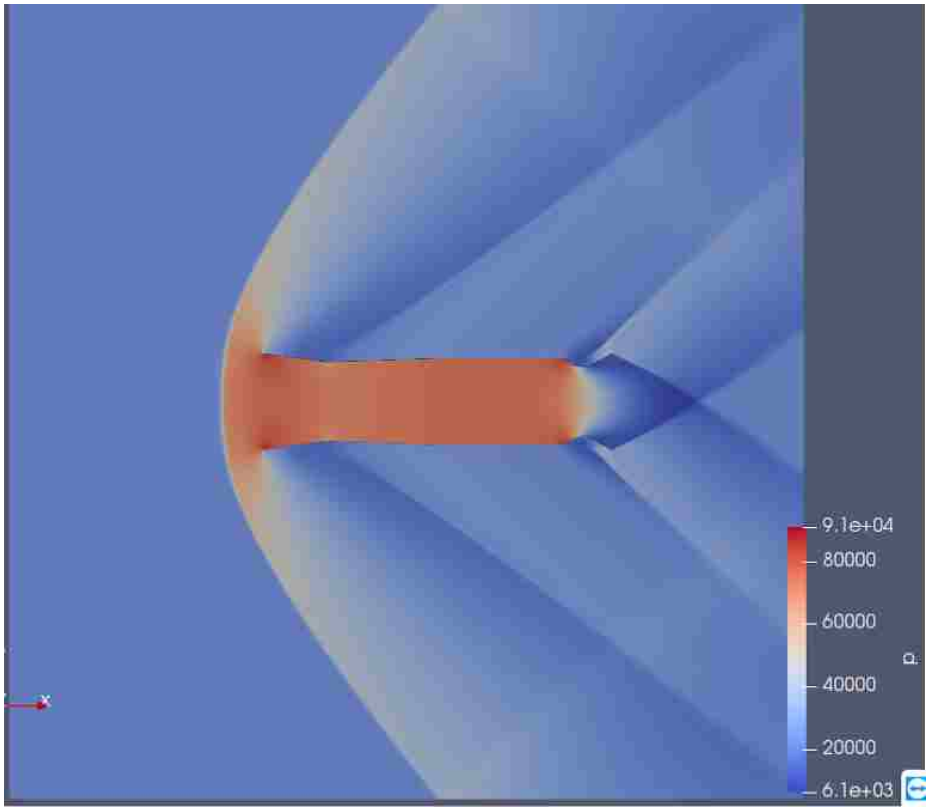


(e) M=1.6(Non-Perforated)

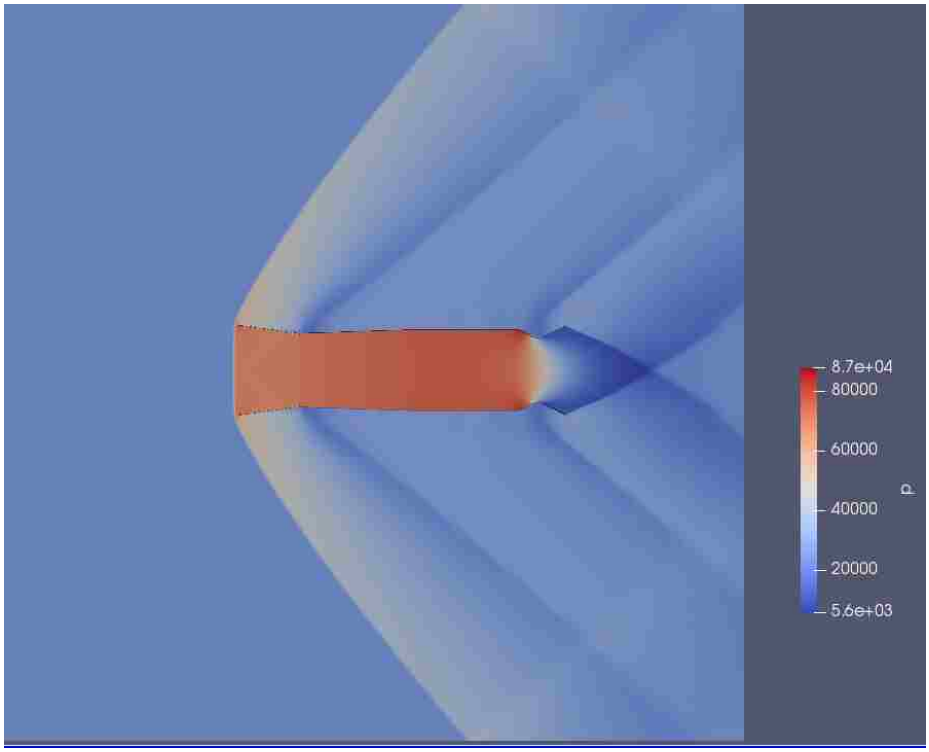


(f) M=1.6(Perforated)

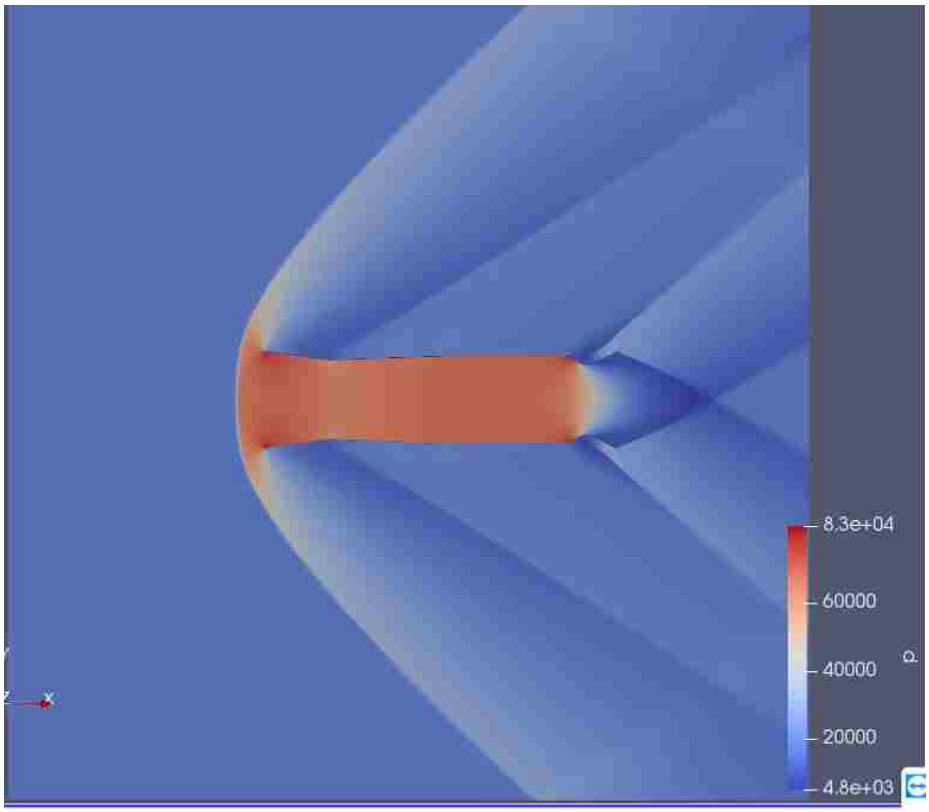


(g) M=1.8(Non-Perforated)

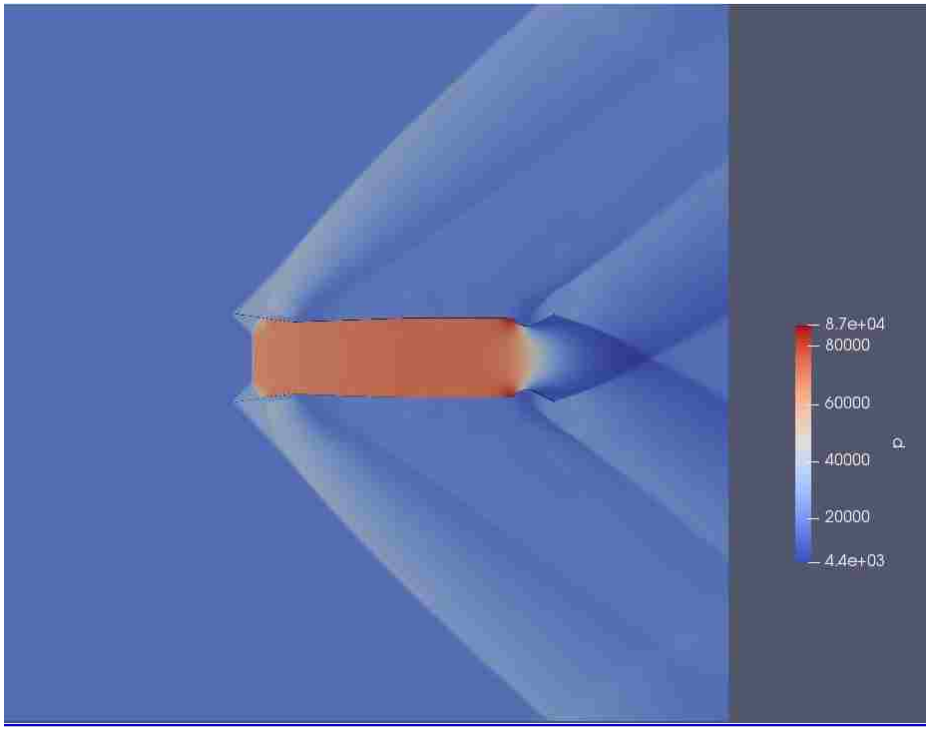


(h) M=1.8(Perforated)

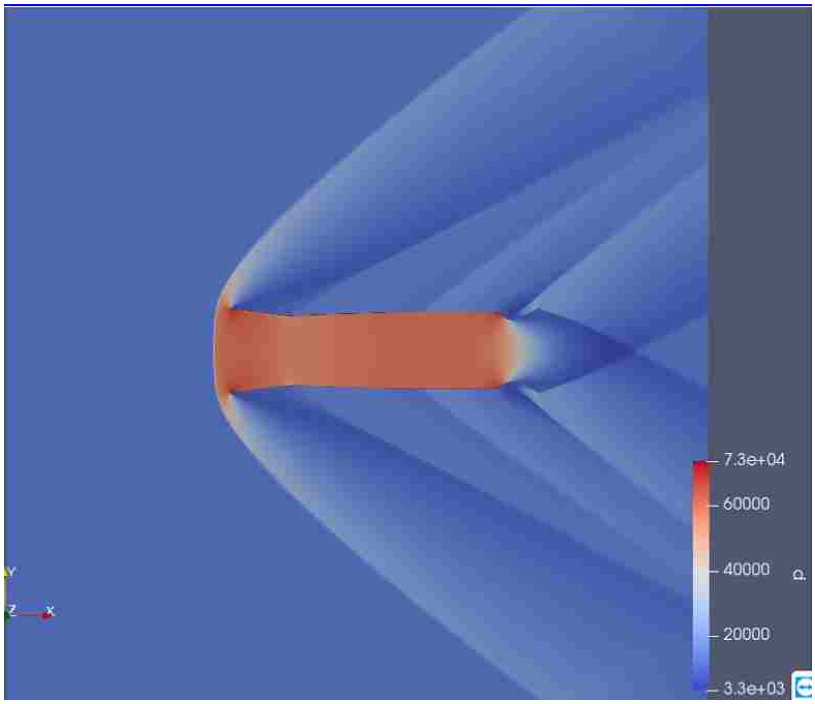


(i) M=2.0(Non-Perforated)

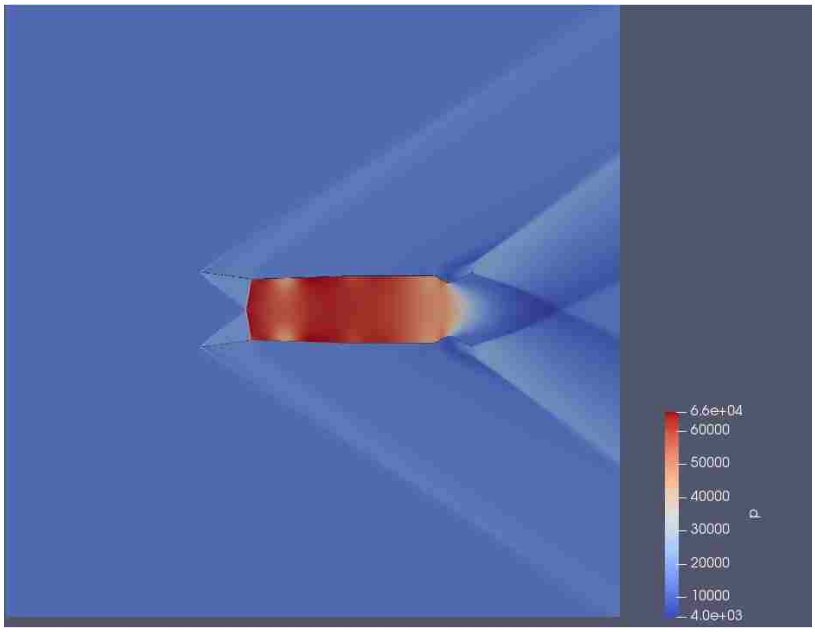


(j) M=2.0(Perforated)

Figure A.1: Contours of Pressure Distribution performed by *sonicFoam* of Supersonic Flow Over Diffuser for incoming supersonic flow from (a) Mach=1.2 for non-perforated diffuser, (b) Mach=1.2 for perforated diffuser, (c)Mach=1.4 for non-perforated diffuser ,(d)Mach=1.4 for perforated diffuser, (e) Mach=1.6 for non-perforated diffuser,(f) Mach=1.6 for perforated diffuser, (g) Mach=1.8 for non-perforated diffuser, (h)Mach=1.8 for perforated diffuser, (i) Mach=2.0 for non-perforated diffuser and (j)Mach=2.0 for non-perforated diffuser.

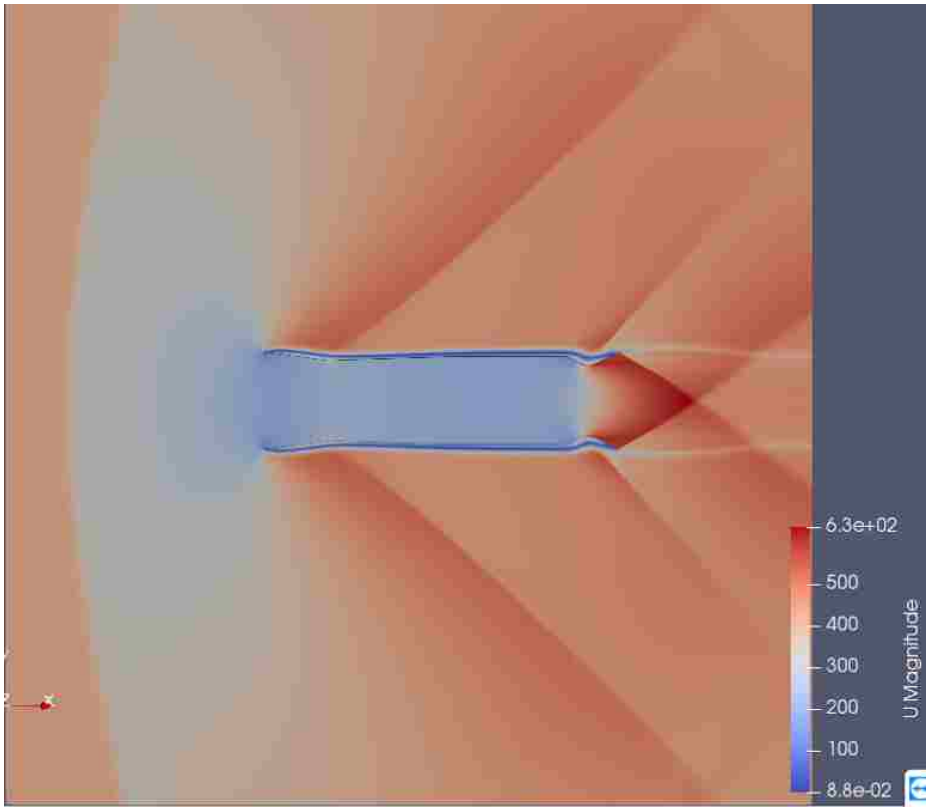


(a) M=1.2(Non-Perforated)

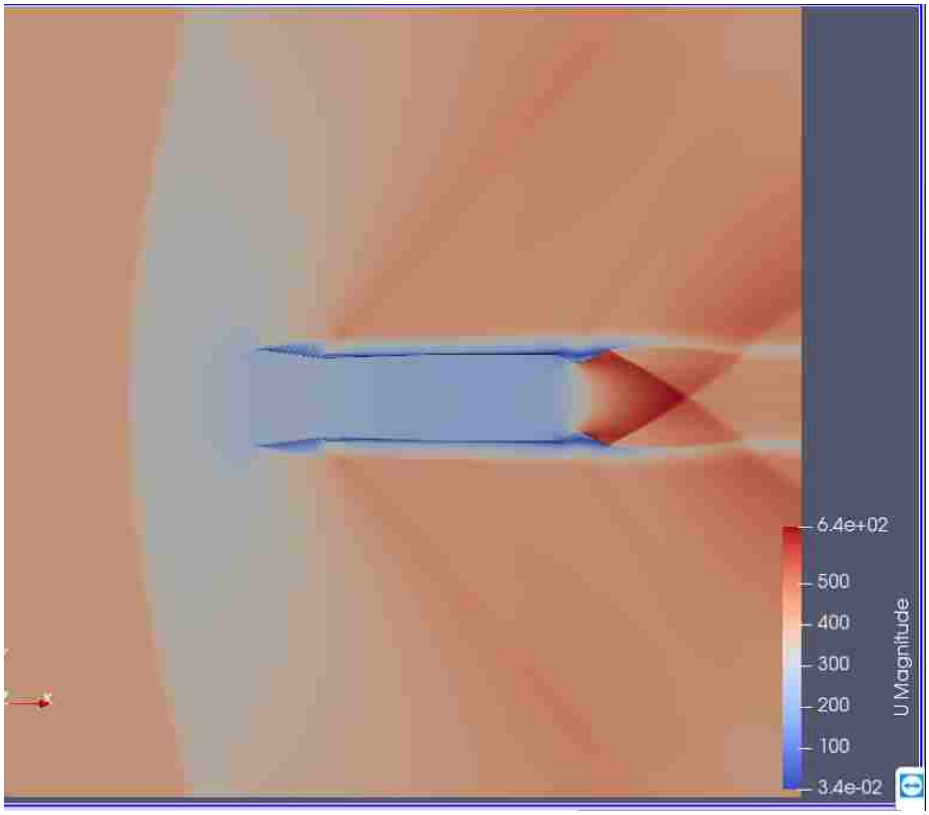


(b) M=1.2(Perforated)

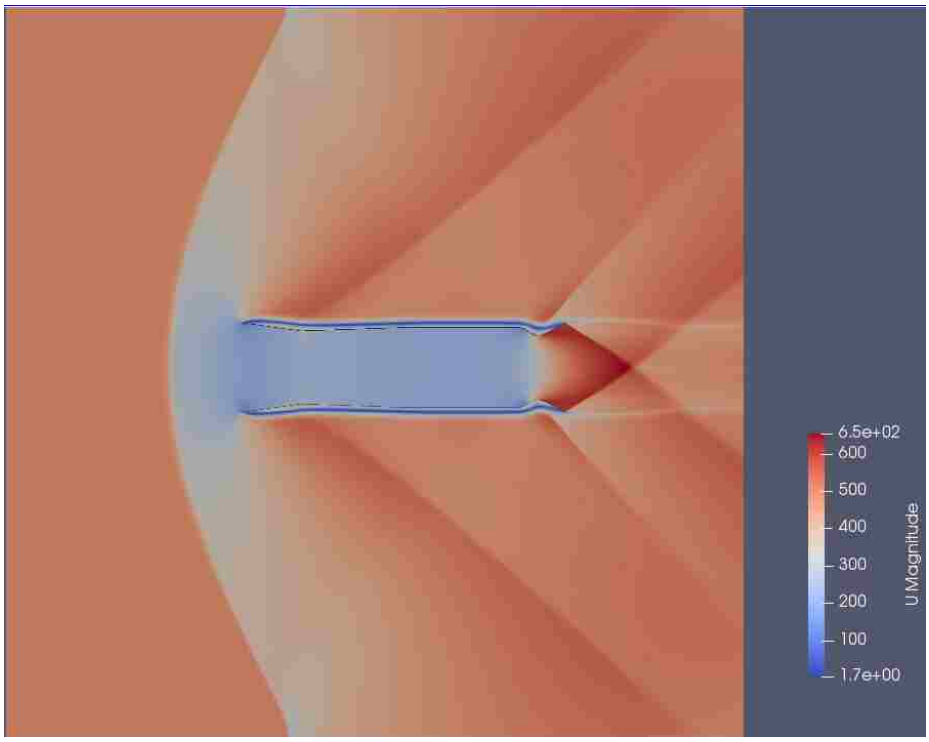


(c) M=1.4(Non-Perforated)

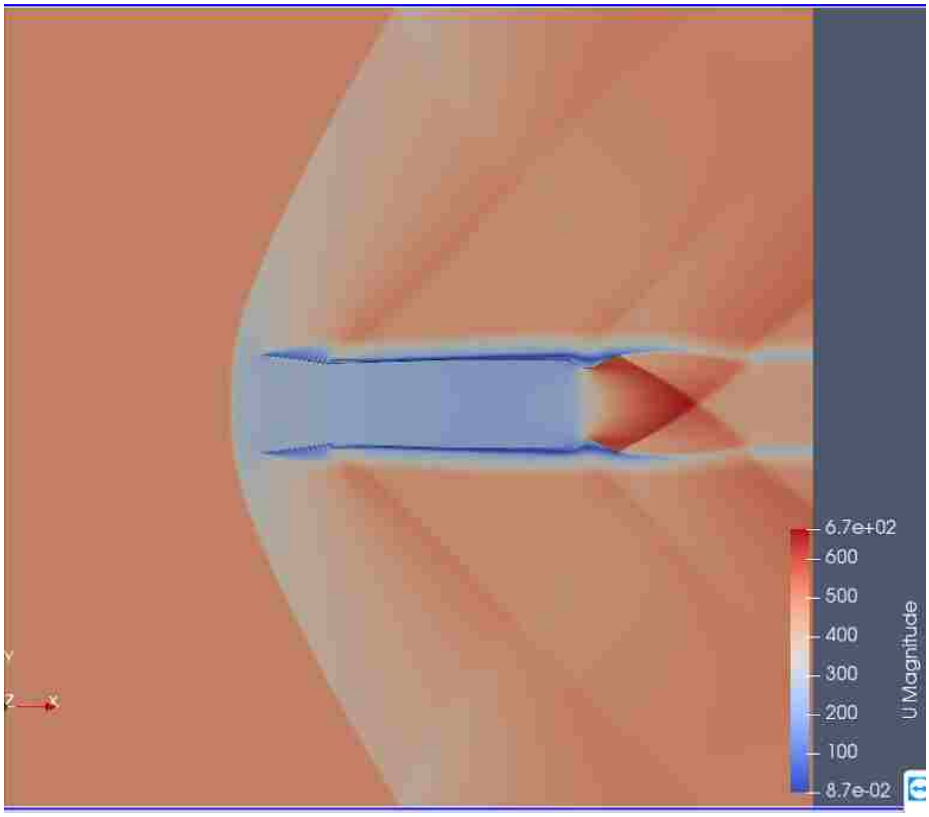


(d) M=1.4(Perforated)

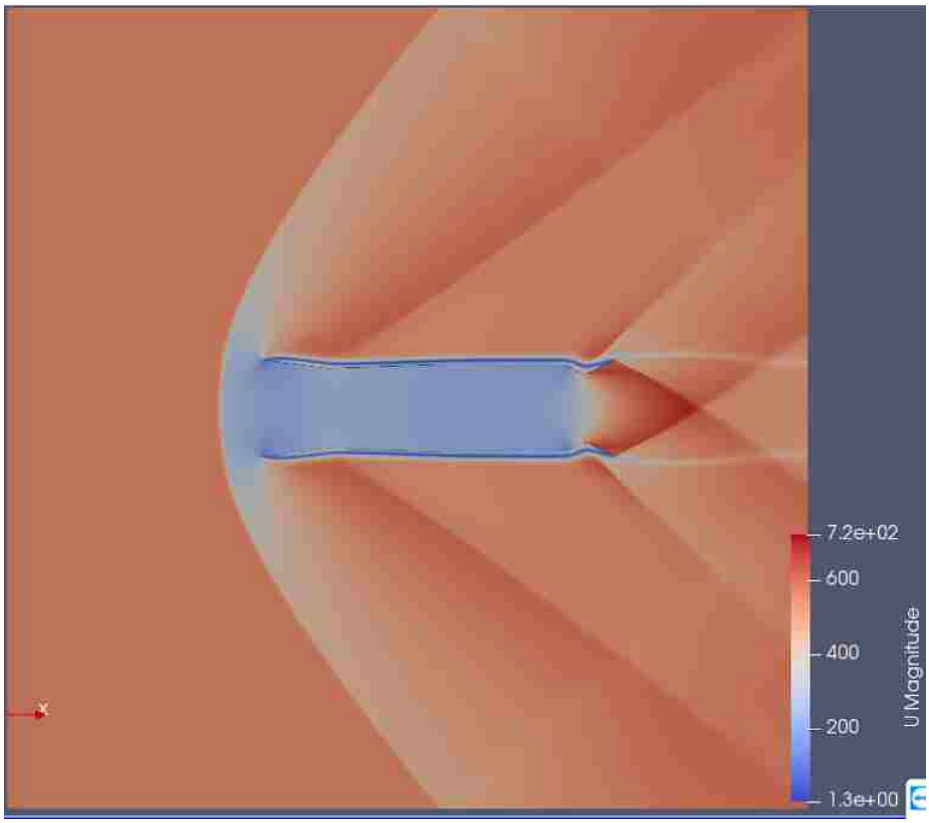


(e) M=1.6(Non-Perforated)

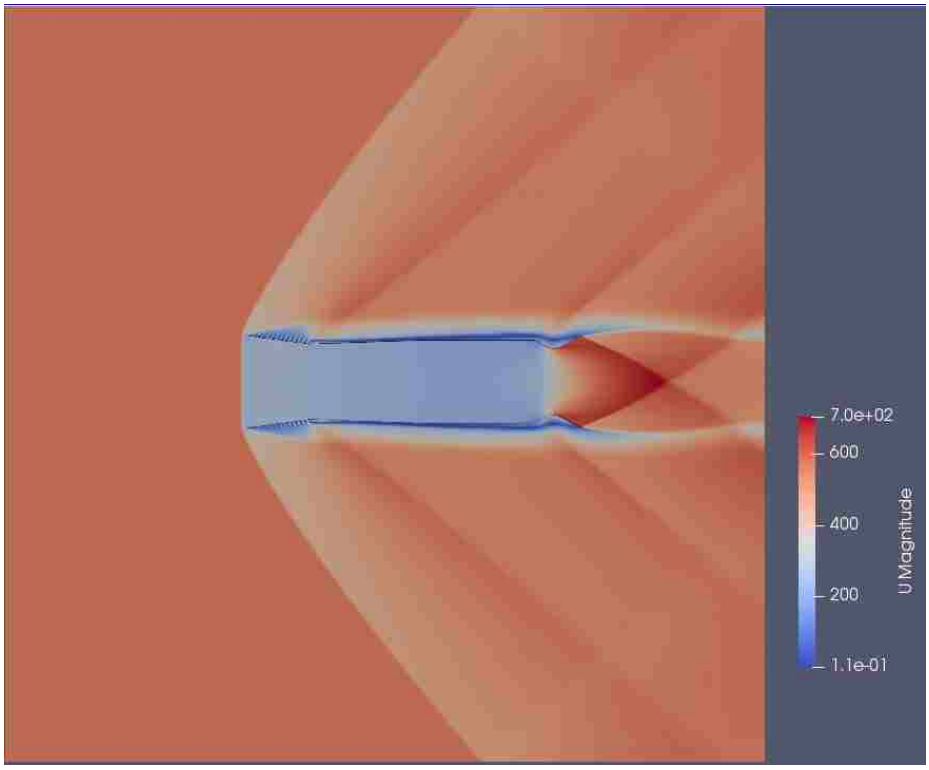


(f) M=1.6(Perforated)

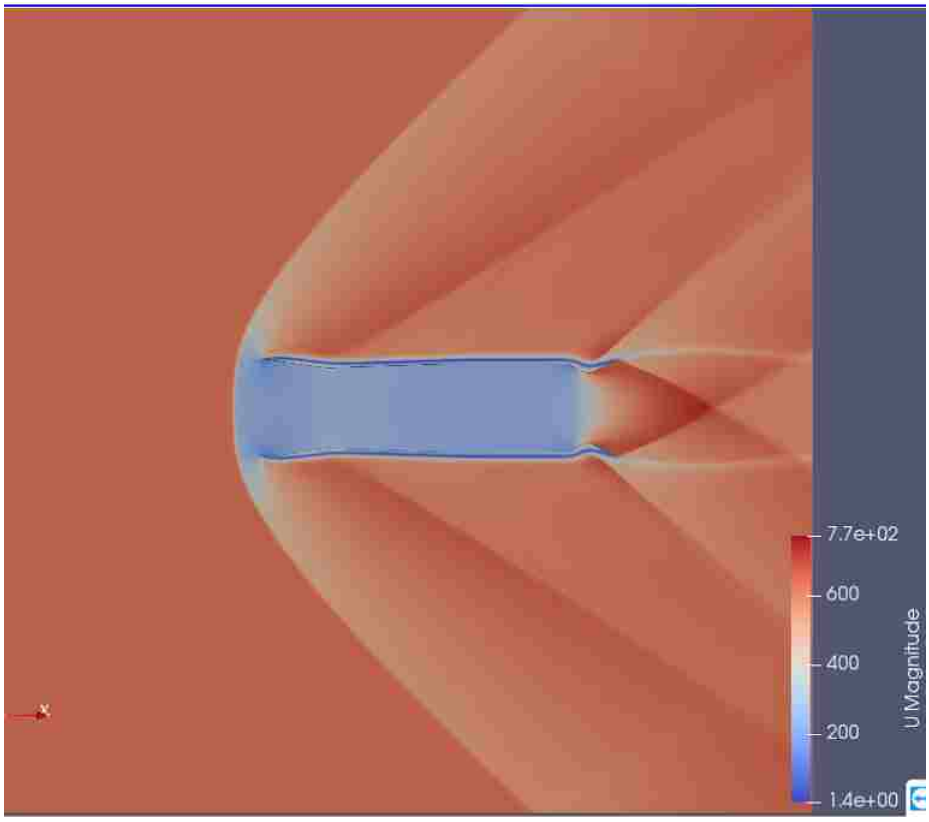


(g) M=1.8(Non-Perforated)

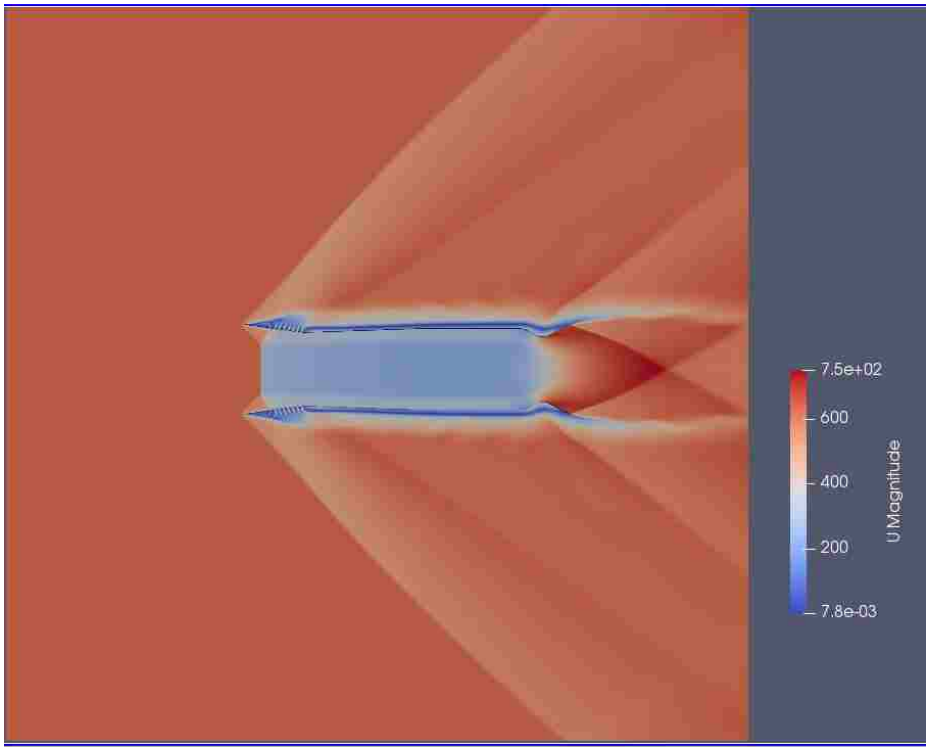


(h) M=1.8(Perforated)

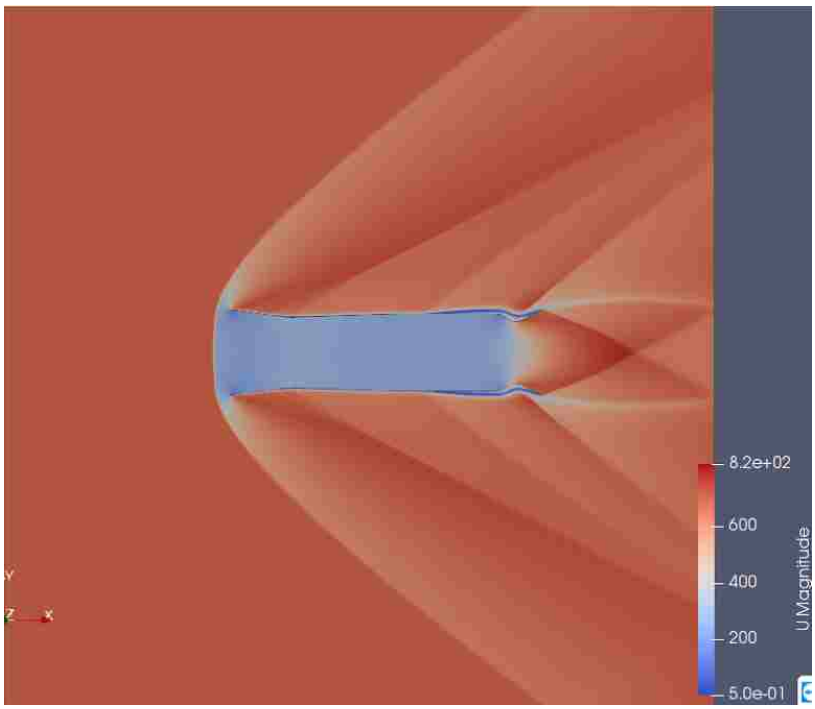


(i) M=2.0(Non-Perforated)

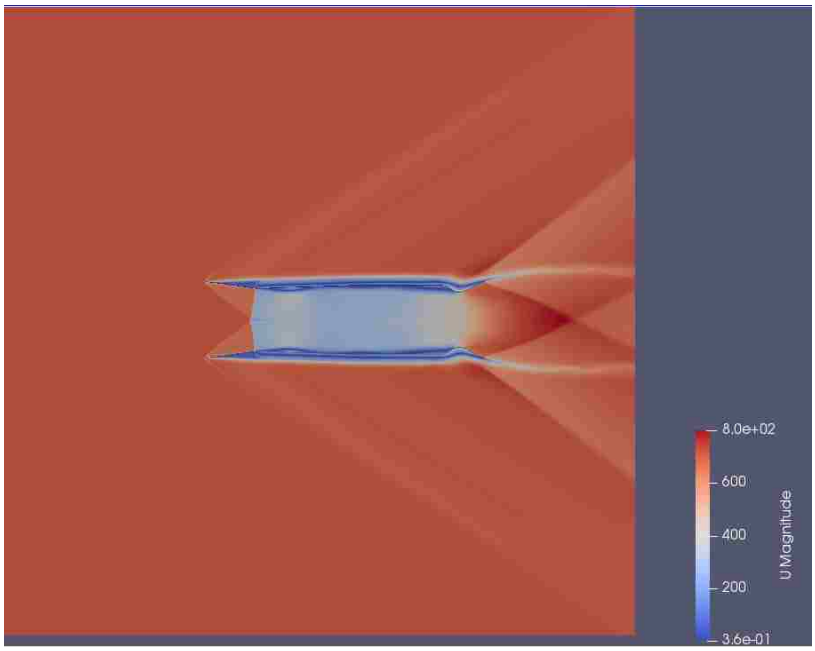


(j) M=2.0(Perforated)

Figure A.2: Contours of velocity Distribution performed by *sonicFoam* of Supersonic Flow Over Diffuser for incoming supersonic flow from (a) Mach=1.2 for non-perforated diffuser, (b) Mach=1.2 for perforated diffuser, (c)Mach=1.4 for non-perforated diffuser ,(d)Mach=1.4 for perforated diffuser, (e) Mach=1.6 for non-perforated diffuser,(f) Mach=1.6 for perforated diffuser, (g) Mach=1.8 for non-perforated diffuser, (h)Mach=1.8 for perforated diffuser, (i) Mach=2.0 for non-perforated diffuser and (j)Mach=2.0 for non-perforated diffuser.

# Biography

Chuwei Chen was born in Langfang, China in May.6, 1993. He completed his bachelor of Engineering degree in Thermal and Power Engineering Jilin University. Afterwards he entered the The P.C.Rossin College of Engineering and Applied Science at Lehigh University to persue his his Master of Science degree.